Aalto-yliopisto
Aalto-universitetet
Aalto University

Master's Programme in Mechanical Engineering

Investigating the In-Plane Properties of the Semi-Regular Square-Triangle Lattice

---

Rashed Moradi

Master's Thesis 2020


Aalto-yliopisto
Aalto-universitetet
Aalto University

Aalto-yliopisto
Aalto-universitetet
Aalto University

Author Rashed Moradi

Title of thesis Investigating the In-Plane Properties of the Semi-Regular Square-Triangle Lattice

Programme Master' Programme in Mechanical Engineering

Major Solid Mechanics

Thesis Supervisor Assistant Professor (Tech) Luc St-Pierre

Thesis advisor (s) Assistant Professor (Tech) Luc St-Pierre

Date 14.11.2020 **Number of pages** 46 + 8 **Language** English

Abstract

The in-plane properties of the Semi-Regular Square-Triangle lattice structure (SST) were investigated under axial and shear load scenarios. The importance of this study was focused on the variation of the in-plane mechanical properties of the lattice as a function of the relative density increments between 0.001 and 0.2. Finite element analysis (FEA) and analytical modelling methods were used to obtain reliable results for the in-plane mechanical properties of the tessellation, including elastic modulus, shear modulus, compressive strength and shear strength. Therefore, these outcomes have been compared with the results obtained for other known stretching dominated lattices. The results of the comparison between FEA and analytical modelling methods showed that they were in good agreement and closely matched, indicating that these are very powerful techniques to study the in-plane mechanical properties of the lattice. The results of the study revealed that the lattice had the lowest stiffness compared to other known lattice structures. In addition, the SST lattice had a higher elastic buckling strength characteristics than the square, triangular and mixed cells and the lowest plastic compressive yielding strength compared to others. In relation to the effective shear modulus, the lattice was found to be superior to the mixed and square lattice topologies. In relation to the aspect of plastic shear yielding strength the lattice was superior to the square and mixed cells, inferior to those of the kagome and triangular lattice topologies.

Keywords Tessellations, Lattice materials, Finite Element Analysis, Analytical modelling, Axial loading, Shearing loading, Stiffness, Strength, Tessellation material, Mechanical properties.

Table of Contents

Preface

This master's thesis was completed in the Aalto University, department of Mechanical Engineering and focused on the study of the SST Lattice properties. I would especially like to thank Professor Luc St-Pierre for suggesting an interesting and outstanding topic, as well as for his patient and tireless support during the project and in difficult times when we were faced with the pandemic COVID 19. I might not have been able to complete my master thesis without his help and support. Furthermore, I would like to thank the staff and lecturers of Aalto University, who provided me with a lot of valuable scientific content.

Finally, I wish to thank my wife for all her help, understanding and commitment during many phases of completing my master thesis.

14. November. 2020

Rashed Moradi

Symbols

$\bar{\rho}_{crit}$	Critical relative density
A_s	Total area of strut
A_u	Area of unite cell
E_s	Young's modulus of the material that used in lattice
b_n	Number of struts in structure
$\bar{\rho}$	Relative Density of Lattice
σ_{Ts}	Tensile strength
σ_{el}	Elastic buckling stress
σ_{ys}	Yield stress
τ_{el}	Shear buckling stress
Δ	Prescribed displacement in shear loading case
B	Stiffness coefficient
H	Height of unit cell
A	Constant of Relative Density
C	Compressive buckling strength coefficient
D	Compressive plastic yield Strength coefficient
M	Shear modulus coefficient
N	Shear buckling strength coefficient
S	Shear plastic yield strength coefficient
W	Width of unit cell
Z	Nodal connectivity
b	The Out-of-plane depth
j	Number of joint in structure
l	Length of Lattice Element
n	End constraint factor
t	Thickness of lattice element
v	Poisson's ratio
δ	Prescribed displacement in axial loading case
σ	Axial Stress
τ	Shear stress

Abbreviations

FEA	Finite Element Analysis
FRP	fiber-reinforced plastics
GFRP	Glass-Fiber Reinforced Plastics
SSTL	Semi-Regular Square-Triangle Lattice
2*D*	2 Dimensional
3*D*	3 Dimensional

1 Introduction

Lightweight materials offer extensive alternative potential for developing a unique combination of material properties. As a result of these efforts, many novel materials have been developed in recent decades as lightweight structures that are appropriately stiff, strong and light. (Deshpande et al. 2001). Therefore, they could be widely used for many important applications, including car and aerospace engineering. Many attempts have been made to find a better solution to obtain an optimum material for various projects, including producing engineered fiber-reinforced plastics FRP and innovative metal alloys.

In the early $1940s$, the polymer materials were used in conjunction with the glass-fiber reinforced plastics GFRP in aircraft technology, while wood and canvas materials were widely used as the lightweight sandwich structures in similar technologies.

In the $1950s$, the development of superalloys such as nickel, heavily alloyed iron and cobalt became the centre of scientific and engineering research, providing an exceptional range of alloys capable of supporting loads at temperatures above $1200\ °$. Thus, the spectrum of their applications was extended to other fields, particularly those in chemical and petroleum engineering (Fleck et al. 2010).

Moreover, many unique materials with a combination of properties were developed in the $1960s$ when carbon fiber and aramid first introduced (Fleck et al. 2010). In principle, the properties of these materials depend on the direction and quantity of fibers inside the plastic. Fiber-reinforced plastic material could be modified for using inside the lightweight sandwich composite. They require a lightweight material because they are not very suitable to use as core material (Davies, 2015).

In the early $1990s$, the importance of nanotechnology was accepted and carbon nanoparticles were used to reinforce vehicle tyres. The use of dispersed precipitates offered an increase in the strength of aerospace light alloys.

In recent years, the research centre has focused on the discovery of novel materials with aspects of low density and high strength. Many approaches have evolved to fill gaps in the spaces material properties, including manipulating of chemistry, manipulating of microstructure and control of architecture to create the hybrid material-combinations of materials or of material and space in configurations and with connectivity that provide improved performance (Fleck et al. 2010). Figure 1.1 depicts the stiffness and strength properties of different materials, as the figure indicates that there will be still a great need to fill the gap in the material space with novel materials that have high strength and low density properties.

1.1 Classification of Lattice Materials

One of the optimal solutions to overcome this need is to find materials with high strength and low density. Lattice materials, which consists of periodic arrangements of interconnected struts, have developed into as a new class of engineering materials (Zok, 2019). Lattice materials offer the possibility to select the most favourable with high strength and low density from a designed structure. Due to their great potential for improvement, they can be manipulated to obtain low

density and high strength properties in their parts of the structure. To achieve the above mentioned, a lattice material structure could be created with light materials and thick fragments, or perhaps made with a small amount of a strong material.

The structure of a periodic lattice material is defined by a set of features that describe the lattice and the constituent lattice elements, in particular struts and nodes (Zok, 2019).The topology of the lattice material structure plays an important role in defining its property, which can be described in $3D$ or $2D$ structures. Periodic planar lattices be separated into three different classes based on their topology characterization, including regular, semi-regular and demi-regular tessellation. In the subsections, these various classes of lattice material and their unique topology are briefly discussed.

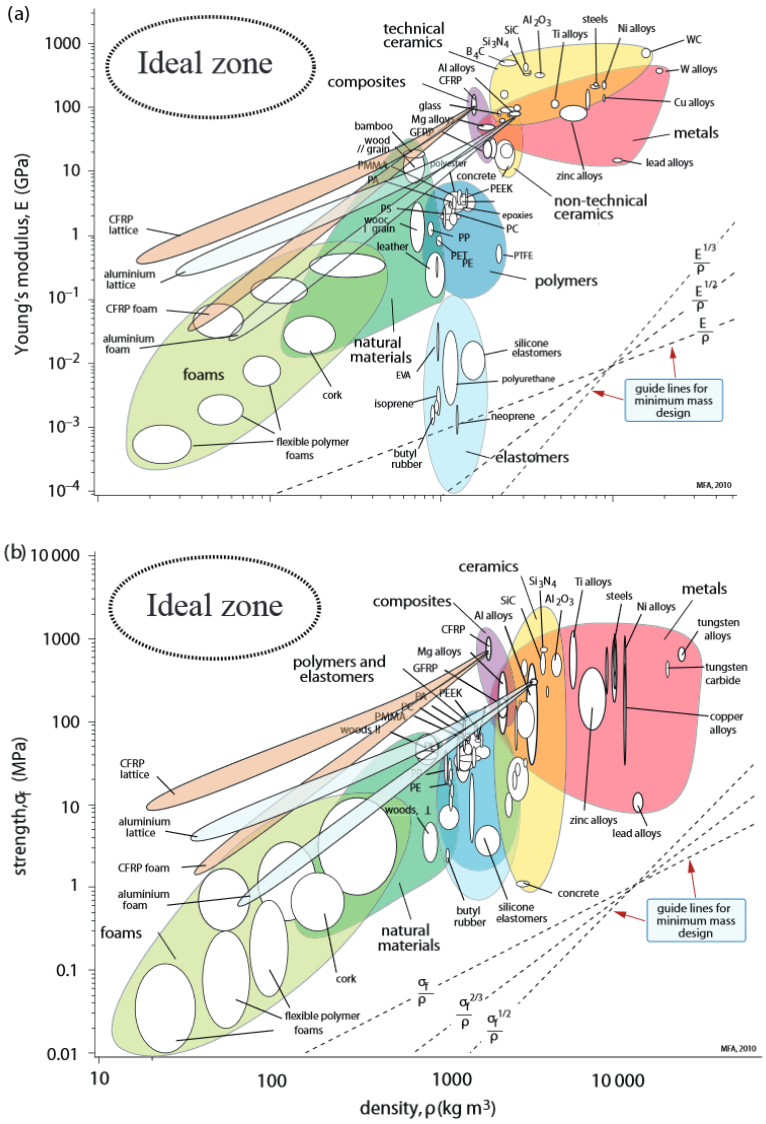

Figure 1.1: Strength and stiffness properties of various material compared to density, which depicts that the development of lightweight materials is highly necessary and the area of material properties with high strength and low density has some room for improvement (Fleck et al. 2010).

1.1.1 Regular Tessellation

Regular tessellation is developed by repeating a regular polygon, and in this type of tessellation, each vertex can be mapped to each vertex figure by symmetry operations that are transitive (Gomez-Jauregui et al. 2012). A regular tessellation is formed so that all its sides and internal angles are equal. As figure 1.2 shows, there are three different types of regular-tessellation that can be created: triangular, hexagonal and square cells. Regular-tessellation is used in the structure of regular lattices and their properties can be applied to help and facilitate the process of manufacturing and designing lightweight materials.

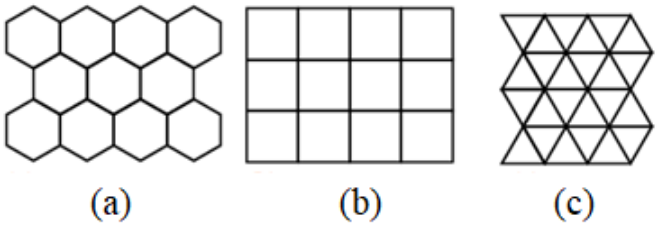

Figure 1.2: Regular tessellation: (a) hexagonal, (b) square and (c) triangle.

1.1.2 Semi-Regular Tessellation

Semi-regular tessellations are known as Archimedean, which contain regular polygons together with a different number of edges that connected with each vertex and respect the same or a similar arrangement obtained by translations, rotations, and reflections (Gomez-Jauregui et al. 2012). The semi-regular tessellation is developed with two or more regular polygons, as opposed to the regular lattice, which contains only one regular polygon. As Figure 1.3 demonstrates, it has been shown that there are only eight possible semi-regular tessellation (H Martyn et al. 2007, Critchlow, 2000 and Branko Grünbaum et al. 2019). Regular and semi-regular tessellation are arranged in such a way that they have similar nodal connectivity.

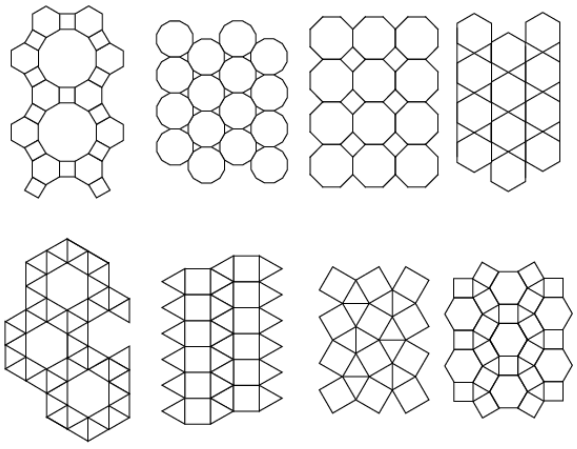

Figure 1.3: Series of semi-regular tessellation geometries.

1.1.3 Demi-Regular Tessellation

Demi-regular or other tessellation materials are really difficult to define, and at some points they can be described as a tilting of eight semi-regular and three regular lattice materials, which is not a very accurate description. In all their configurations, the arrangement of the vertices is not unique and their regular polygons converge in different ways (Gomez-Jauregui et al. 2012). The number of other tessellation is determined to be fourteen, which is also not very accurate (H Martyn et al. 2007). As Figure 1.4 depicts, a demi-regular tessellations is created by arranging a series of squares and equilateral triangles that can be changed up and down to form square lines that are connected to each other. Krötenheerdt initially numbered these demi-regular tessellations twenty (Branko Grünbaum et al. 2019). So we can conclude that mathematicians do not agree on their exact definition and as opposed to semi-regular lattices, not all nodes have the same nodal connectivity (demi-regular lattices have 2 values of nodal connectivity).

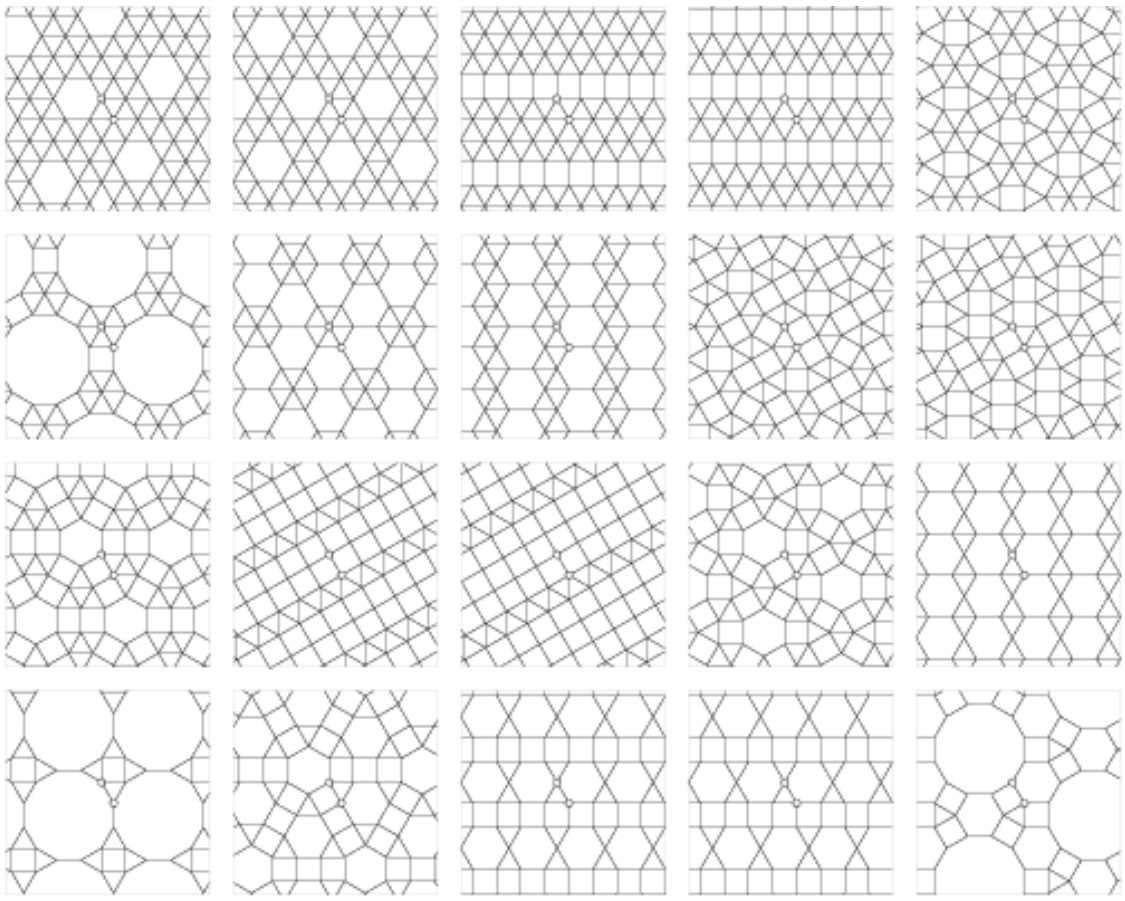

Figure 1.4: Series of determining demi-regular tessellation.

1.2 Scope of Master's Thesis and Methodology

The focus of this current study is to investigate the in-plane mechanical behaviour of a unique semi-regular tessellation called as the SST lattice. This study deals with the investigation of the in-plane properties of the SST lattice topology based on two different scenarios, including shear and axial loading for relative density increments between 0.001 and 0.2. Moreover, the in-plane properties of this lattice are modelled and analytically developed based on simple beam and truss theories in both loading cases. The $2D$ geometry of the lattice was generated using the commercial software Abaqus and then investigated in both scenarios using the FEA technique. The results of the analytical modelling approach are compared graphically and numerically with the outcome of the FEA technique. Moreover, the relative density constant of the SST lattice structure is calculated and then compared with those other well-known lattices such as kagome, square, triangular, mixed lattices. Finally, this paper focuses on the graphical and numerical comparison of the in-plane mechanical properties of known lattice structures with the SST lattice in terms of elastic modulus, compressive strength, shear modulus and shear strength.

1.3 Structure of the Thesis

The content of the present study is divided into seven chapters. Chapter 2 contains a brief description of the lattice mechanical characterization under loading conditions as well as a definition of the relative density in connection with other known lattices and the SST lattice. Furthermore, this chapter focuses on the definition of stretching and bending domination in the lattice and the mechanical behaviour of the lattice respect to elastic stiffness, compressive strength, shear modulus and shear strength shear and axial loading conditions. Chapter 3 shows a series of calculations to obtain a result in relation to the analytical modelling approach, which is based on the beam theory and also determines the in-plane properties of the lattice in both scenarios. Chapter 4 includes the investigation of the lattice mechanical behaviour with the FEA approach by performing a series of simulations in both loading cases. Chapter 5 discusses the differences in the results obtained from FEA and analytical modelling methods and also compare these outcomes with other known lattices. Finally, chapter 6, 7 and 8 contain the final remarks of the current study, available references and further details (appendices).

2 Literature Review

Lattice materials are the optimal choice for developing a design structure with a combination of excellent strength and stiffness properties and low weight. This chapter briefly explains the importance of understanding the basic concept of relative density and a unit cell of the lattice material structure. Moreover, the following subsections introduces the mechanism of stretching and bending that prevails in lattice material under shear and axial loading, together with the fact that the mechanical characterization of the lattice structure is very similar to that in truss structures, so that the similar mathematical approach could be used to determine the structural forces on the bars and the displacement in the lattice joints. The study of this chapter focuses on the derivation of dimensionless equations for the in-plane mechanical properties of the lattice structure, including stiffness, axial compressive strength, shear modulus and shear strength. Moreover, the value of in-plane mechanical property constants for other known lattice topologies is discussed in Table 2.2.

2.1 Unit Cell in Lattice Materials

The structure of the lattice material is described as a truss, lattice, cellular and reticulated, which consists of a large number of uniform lattice elements such as bar, beam and slender and was developed by tessellating a unit cell consisting of a few lattice elements throughout the entire space (Fleck et al. 2010).

The calculation process of a lattice material structure can be facilitated by simplifying its unique topology. As Figure 2.2 shows, the topology of a large lattice material can be simplified into a smaller part called as a unit cell. These unit cells can be stacked to create a large lattice structure. A structure of a lattice could be assembled by connecting these periodic unit cell boundaries at the end of each lattice element to the adjacent unit cell. It is important to note that the unit cell has to be selected by cutting across a lattice element and not along that. To the best of our knowledge, the computational time and cost of FEA simulation could be decreased with simplifying complex forms of tessellation to a unit cell. In this current study the unit cell of the SST lattice was selected, as shown in Figure 2.1.

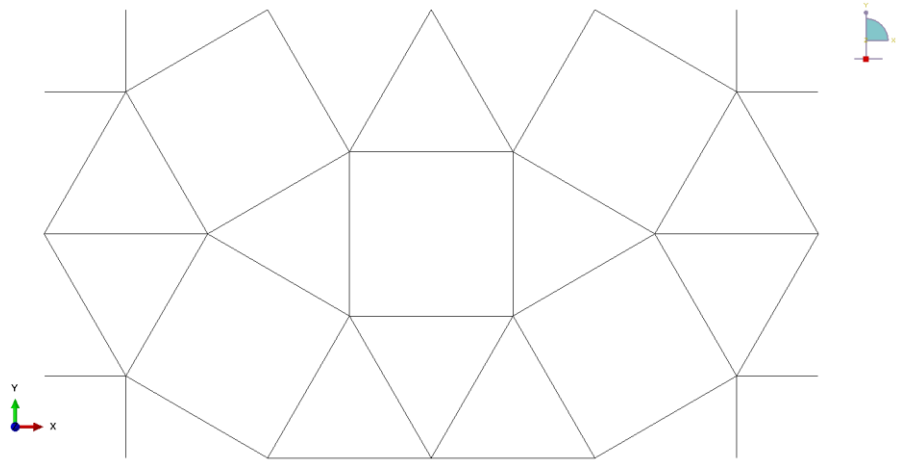

Figure 2.1: The SST lattice unit cell.

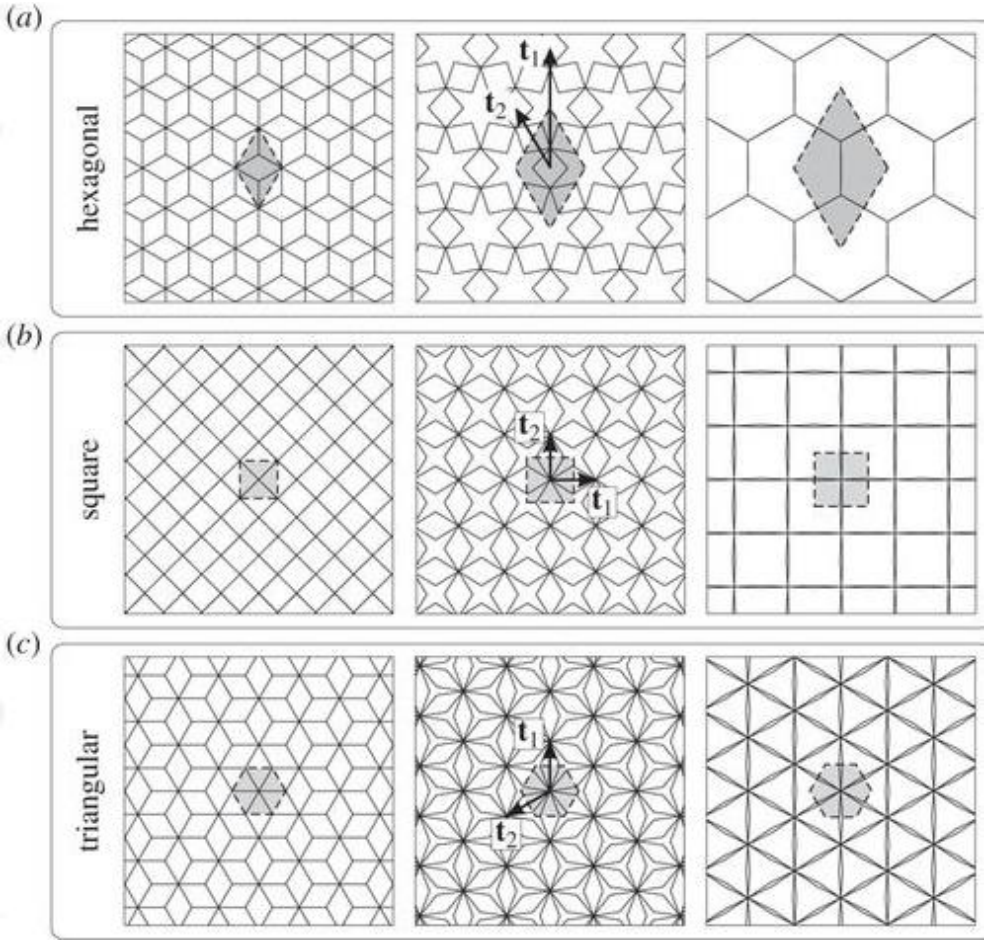

Figure 2.2: Periodic cellular lattices: (a) hexagonal (b) square (c) triangular (Cabras and Brun, 2014).

2.2 Relative Density of Lattice

The investigation of lattice materials and their mechanical properties requires a deep familiarity with the concept of relative density. Relative density is defined as the ratio of the lattice material to the solid material from which the lattice structure is created. On the other hand, the relative density can be expressed in terms of the length of the lattice element and the thickness:

$$\bar{\rho} = A\frac{t}{l} \tag{2.1}$$

A is known as a constant of relative density, which is actually based on the topology of the lattice. Table 2.1 shows some of the relative density values in several known lattice materials.

The relative density of the SST lattice is calculated in chapter 3 of this current study and then compared with the values obtained for various types of cell structures, as shown in Table 2.1.

Table 2.1: Constant of relative density A for various types of lattice topologies (Wang and McDowell, 2004).

Lattice Topology	*A*
Kagome Cell	$\sqrt{3} = 1.7321$
Triangular Cell	$2\sqrt{3} = 3.4641$
Square Cell	2
Mixed Cell	$2 + \sqrt{2} = 3.4142$

2.3 Stretching and Bending Dominated in Cellular Materials

The mechanical properties of a lattice material are analysed with the theory of the simple beam, since the cells of the lattice are considered as very thin elements. Therefore, the theory of the Timoshenko's beam can be applied to study the mechanical properties of the SST lattice. With respect to the deformation mechanism, material lattices are divided into various collections, including bending and stretching dominated mechanisms. In the scenario dominated by bending, the bars are deformed by bending loading, while in the case of the stretching dominated, the lattice elements of the structure are stretched by either compressive or tensile loading. In recent years, many attempts have been carried out to study the lattice system topologies and the mechanical aspects associated with them, in which researchers agreed that the strength and stiffness of material lattices dominated by either bending or stretching can be defined as the following relationships (Gibson and Ashby, 2010), for stretching dominated lattice topology:

$$E \propto \overline{\rho}^{b} \tag{2.2}$$

Where $b = 1$

$$\sigma_y \propto \overline{\rho}^{b} \tag{2.3}$$

Hence, $b = 1$

For bending dominated lattice topology:

$$E \propto \overline{\rho}^{b} \tag{2.4}$$

The value of $b = 2$

$$\sigma_y \propto \overline{\rho}^{b} \tag{2.5}$$

Where $b = 1.5$

The above mathematical relationships indicates that at a low value of relative density, the stretching dominated lattice is roughly about three times stronger and ten times stiffer than the bending dominated lattice material. The study shows that the stretching dominated lattice topology offers greater stiffness per unit weight than the bending dominated case (Chopra, 2009). This remarkable distinction is more likely to be found in the case of low relative densities.

As shown in Figure 2.3, there are two various structural mechanisms, so-called pin-joint bars, which behave differently in comparison to each other. In these types of mechanisms, the bars resist axial loading, either tensile or compressive in the structure as the pins rotate (Fleck et al. 2010).

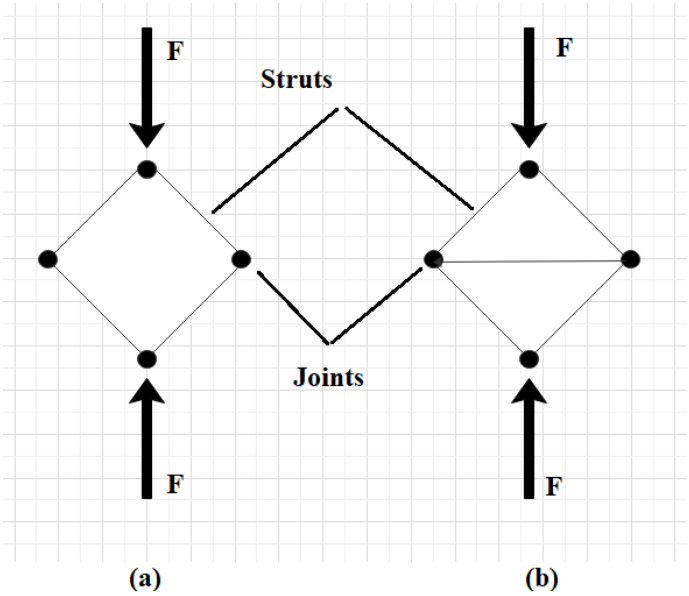

Figure 2.3: (a) A structure affected by bending dominated mechanism. (b) A structure affected by stretching dominated mechanism.

The mechanical structure of the Figure 2.3 a could not resist against the axial force, so that the bar finally bent. In contrast, the bar in Figure 2.3 b is able to withstand the axial force because there are either compressive or tension forces within the frame. When the situation changes in such way that the joints become rigid enough for the frame, as shown in Figure 2.3 a the loading force creates a bending moment at the joints and causes deformation of the frame. In the latter case, however the frame only creates an axial load within the bars (Fleck et al. 2010). The structure of pin-joints have been studied in detail with (Maxwell, 1864) as he mentioned the fact that the $2D$ frame does not bend when the following equation is satisfied:

$$b_n = 2j - 3 \tag{2.6}$$

The number of the bars can be expressed by the following equation:

$$b_n = \frac{jZ}{2} \tag{2.7}$$

Where j is the number of joints, b_n is the number of bars and Z known as nodal connectivity.

Considering Equation 2.7 for a large system of lattice, the value of $Z = 4$ which is not sufficient because the structure consists of either periodic collapse mechanism or macroscopic strain-

producing mechanism and perhaps both of them (Hutchinson and Fleck, 2006, Pellegrino and Calladine, 1984). A perfectly rigid $2D$ stricture of lattice can be observed in the triangular lattice topology. To achieve perfect rigidity, the structure must have a value $Z = 6$ (Fleck et al. 2010). The SST lattice has some joints with 5 bars and others with 6. So we would expect Z value to be between 5 to 6.

2.4 Review of the Mechanical Properties of Lattice Materials

This study addresses in-plane mechanical properties of the SST lattice in relation to the stiffness and compressive strength, shear modulus and shear strength for both shear and axial loading scenarios. The equations and results obtained can be described as a function of Young's modulus E_s and yield strength σ_y of the parent material.

In this current study, it is assumed that the parent material used in the SST lattice to be linear-elastic-perfectly plastic. The results obtained from the analytical and FEA calculations are expressed in the dimensionless formulas to facilitate comparison between other known with the SST lattices.

2.4.1 Elastic Modulus

Based on the beam theory, the in-plane stiffness of the lattice can be defined by a dimensionless formula as follows:

$$\frac{E}{E_s} = B\bar{\rho}^b \tag{2.8}$$

This equation is related to the lattice topology. B and b are known as stiffness coefficient under uniaxial tensile loading. Equation 2.11 is expressed in a dimensionless form, indicating that the lattice structure obeys the stretch dominated mechanism at $b = 1$ and with $b = 3$ obeys the bending dominated mechanism (Fleck et al. 2010).

2.4.2 Axial Compressive Strength

The elastic buckling strength of the lattice during the uniaxial compression loading condition can be defined in a dimensionless form as:

$$\frac{\sigma_{el}}{E_s} = C\bar{\rho}^c \tag{2.9}$$

C and c are known as coefficients of the elastic buckling strength of the lattice structure under uniaxial compressive loading, which shows that the lattice can buckle elastically.

Moreover, the yield strength of the lattice can be described as the following equation, which is used for the lattice yielding condition:

$$\frac{\sigma}{\sigma_{ys}} = D\bar{\rho}^{d} \tag{2.10}$$

D and d are known as coefficients of the plastic yield strength of the lattice and if $d = 1$, the lattice is affected by the mechanism of stretching dominated while $d = 2$ shows the mechanism of bending dominated. It is important to note that the plastic yielding failure of the lattice structure can only occur under axial tensile condition, whereas in the uniaxial compression condition the lattice would yield at higher relative densities and finally would buckle at lower relative densities. Therefore, by rearranging the equations 2.10 and 2.9 the critical relative density of the lattice can be expressed in the form of a new dimensionless equation, which gives:

$$\bar{\boldsymbol{\rho}}_{\boldsymbol{crit}} = \left(\frac{D\sigma_{ys}}{C\ E_s}\right)^{\frac{1}{c-d}} \tag{2.11}$$

The deformation mechanism of the lattice structure changes at the critical density point in such a way that the elastic buckling strength mode is shifted to the plastic yield strength mode of deformation under compressive axial loading condition.

2.4.3 Shear Modulus

Following the above equations in the previous subsections, the same principle could be applied to generate a non-dimensional form of the equation expressing the shear modulus of the lattice as follows:

$$\frac{G}{E_s} = M\bar{\rho}^{m} \tag{2.12}$$

This equation is related to the lattice topology. Since M and m are known as coefficient for the shear modulus of the lattice under shear loading. Equation 2.12 concludes that when $m = 1$ the lattice obeys the mechanism dominated by strain and at $m = 3$ the structure of the lattice is influenced by the mechanism dominated by bending.

2.4.3 Shear Strength

The buckling shear strength of the lattice during the shear stress can also be defined in a dimensionless form:

$$\frac{\tau_{el}}{E_s} = N\bar{\rho}^{n} \tag{2.13}$$

N and n are known as coefficients of shear the buckling strength of the lattice. In addition, the strength of the lattice can be described as the following equation, which is used for the plastic yield strength of the lattice under shear loading:

$$\frac{\tau}{\sigma_{ys}} = S\bar{\rho}^{n} \tag{2.14}$$

Therefore, the critical relative density of the lattice can be expressed by rearranging the equations 2.14 and 2.13 in the form of a new non-dimension equation as the following:

$$\bar{\boldsymbol{\rho}}_{\boldsymbol{crit}} = \left(\frac{S\sigma_{Ts}}{NE_s}\right)^{\frac{1}{n-s}} \tag{2.15}$$

2.5 Mechanical Properties of Known Lattice Material

Table 2.2 shows the in-plane mechanical properties of various lattice structures. The properties of these lattices are expressed analytically and are compared in Chapter 5 with the analytical results obtained from the SST lattice. The information obtained in Table 2.2 depicts that the kagome and triangular cell is stiffer and has a higher shear modulus compared to other lattice topologies.

Table 2.2: In-plane mechanical properties of different types of known cellular topologies (Wang and McDowell, 2004) (Fleck et al. 2010).

		$\frac{E}{E_s} = B\bar{\rho}^b$		$\frac{\sigma_{el}}{E_s} = C\bar{\rho}^c$		$\frac{\sigma}{\sigma_{ys}} = D\bar{\rho}^d$		$\frac{G}{E_s} = M\bar{\rho}^m$		$\frac{\tau}{\sigma_{ys}} = S\bar{\rho}^s$		
Lattice Geometry	*A*	*B*	*b*	*C*	*c*	*D*	*d*	*M*	*m*	*S*	*s*	*v*
Kagome Cell	$\sqrt{3}$	0.333	1	0.366	3	0.5	1	0.125	1	0.289	1	0.33
Triangular Cell	$2\sqrt{3}$	0.333	1	0.0914	3	0.333	1	0.125	1	0.289	1	0.33
Mixed Cell	$2+\sqrt{2}$	0.369	1	0.029	3	0.369	1	0.104	1	0.207	1	0.146
Square Cell	2	0.5	1	0.103	3	0.5	1	0.0625	3	0.125	2	0.5 vr

In terms of elastic compressive buckling strength the kagome lattice is the strongest. Between these lattices the kagome and square lattices have higher values of plastic yield strength under compressive forces. In addition, the kagome and triangular lattices have the greatest plastic shear yield strength in contrast to other lattice topologies. Unfortunately, the property of elastic shear buckling for other known lattice topologies has not yet been investigated by researchers and is not available.

3 Analytical Modelling

The in-plane mechanical properties of the lattice material can be investigated using two various methods, including FEA techniques and analytical modelling approaches. The results obtained from these investigations are compared in chapter 5 to deepen our understanding of the reliability of the present study. The analytical modelling technique is used to obtain an accurate outcome for the in-plane mechanical properties of the perfect lattice material. This series of calculations is performed using truss and beam theories.

3.1 Relative Density

The unit cell of the SST lattice is illustrated in Figure 3.1. The topology of the lattice structure consists of a periodic of interconnected bars at angles of 0°, 60° and 90° with a length of l. Figure 3.1 schematically shows the angle and the symbols used in the analytical modelling calculation for the lattice. The cross-sectional area of the lattice structure is considered as rectangular geometry.

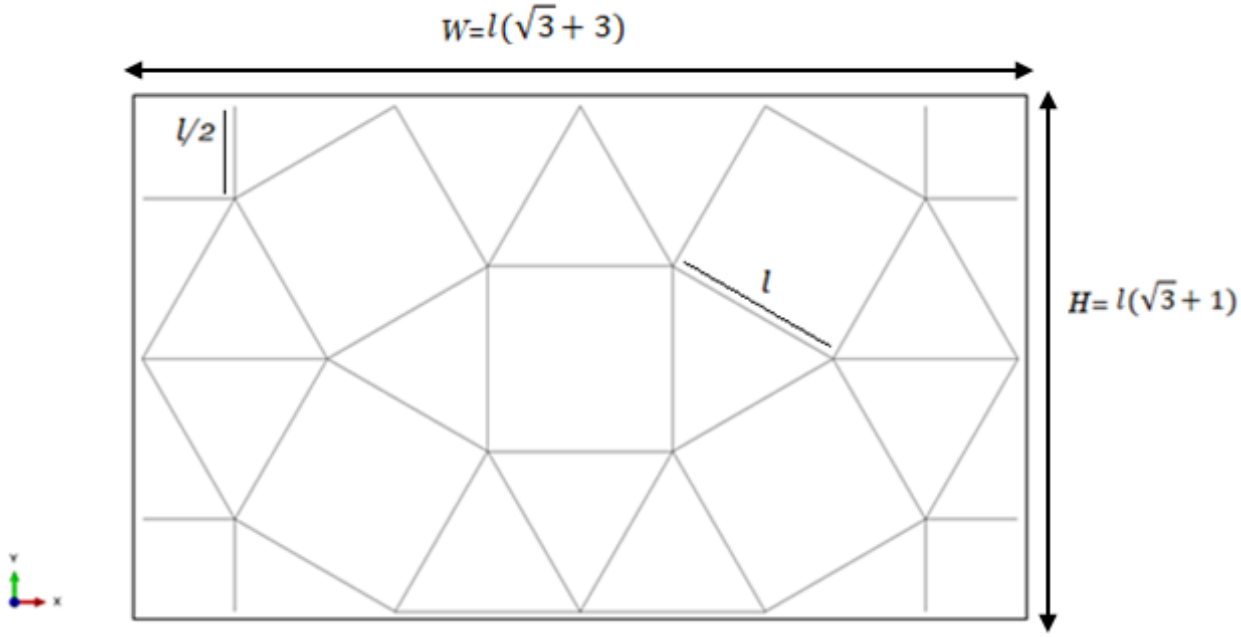

Figure 3.1: Unit cell of the semi-regular Square Triangle SST lattice. The length of the individual bars connected to each other in square and triangular geometries on the lattice is $l = 20\ mm$, since the length of 8 struts located at the corner sides of the lattice is $l/2$ =10 mm.

A series of calculations are performed to obtain the relative density of the SST lattice, the result could be used to study the in-plane mechanical properties of the lattice in upcoming chapters of this work. The relative density of the lattice is determined in the $2D$ scenario by the ratio of the total cross-sectional area of the parent lattice to the total cross-sectional area of the lattice according to Equation 3.1. Thus, the height and width parameters of the lattice are required to

obtain the cross-sectional area of the lattice. The total cross-sectional area of the bars in the lattice can be determined by multiplying the total number of bars 36 with the thickness and length of each bar.

In the end the value of the relative density is given by the following equation:

$$\bar{\rho} = A\frac{t}{l} = \frac{36tl}{HW} = \frac{36tl}{l^2(6+4\sqrt{3})} = 2.7846\frac{t}{l} \tag{3.1}$$

3.2 Elastic Modulus Property under Uniaxial Load

Considering the lattice loaded by a uniform compressive stress as shown in Figure 3.2, the total forces acting on the lattice bars could be determined by applying a series of structural calculations. Due to the symmetry (the two blue lines) there are only 5 unknown bars, which are marked $1-5$. The other bars obey the bending mechanism, so that they make a negligible contribution compared to the others, which are affected by axial tension/compression forces. Considering aforementioned idea, 5 separate equations are required to solve the system as the following:

- The sum of the forces in x and y at node g. This gives 2 equations. See Appendix 1,
- the sum of the force in x at node m,
- the sum of the forces on the upper (or lower surfaces) is equal to σbW and
- the last equation is more complicated; it should be based on the deformation of the unit cell.

Appendix 1 includes this series of structural calculations based on truss theory, which results 5 unknown equations, as shown below:

$$-T_4 - T_2 Cos\,60 + T_3 Cos\,60 = 0 \tag{3.2}$$

$$-T_1 + T_3 Cos\,30 + T_2 Cos\,30 = 0 \tag{3.3}$$

$$T_1 + T_3 Cos\,30 + T_2 Cos\,30 = -\sigma bW/2 \tag{3.4}$$

$$T_5 + 2\,T_3 Cos\,60 = 0 \tag{3.5}$$

$$2T_2 + T_5 = 2T_3 + T_4 \tag{3.6}$$

Following a series of calculations in Appendix 1, the computational solver is used to determine the axial force values for T_1, T_2, T_3, T_4 and T_5. Table 3.1 shows the numerical results and their types of these axial forces.

Table 3.1: The values of the uniaxial forces applied in the system. The uniaxial forces, including T_1, T_2 and T_3 are compression forces, while the remaining are tension forces.

T1	-0.25 σbw	*Compression*
T2	-0,1684 σbw	*Compression*
T3	-0,1203 σbw	*Compression*
T4	0,0241 σbw	*Tension*
T5	0,1203 σbw	*Tension*

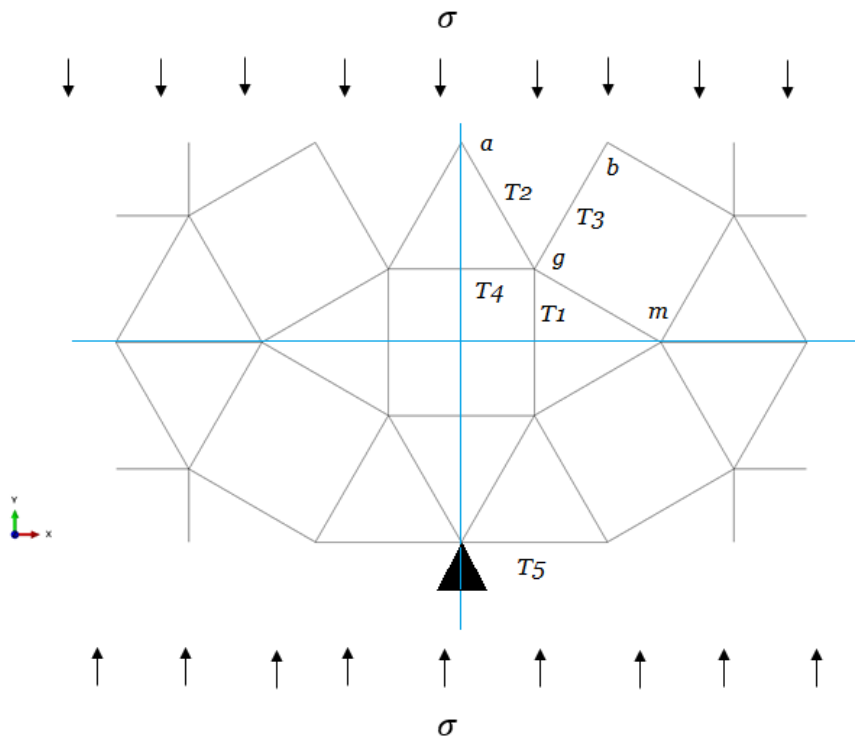

Figure 3.2: Because of the symmetry (the two blue lines) there are only 5 unknown bars, which are marked $1-5$ here. The bars that are not marked obey the bending mechanism so they make a negligible contribution compared to others, which are in axial tension/compression forces.

The investigation of the displacement of the top nodes in the unit cell would be the next step of the analytical modelling calculation. This could be achieved by applying the principle of virtual work, which is being extensively studied by (Krenk and Høgsberg, 2016). This series of calculation is implemented based on truss structure theory and explained in more detail in Appendix 2.

Using the result obtained in the Table 2 in Appendix 2 and inserting these results in Equation 2.4, in Appendix 2 gives the displacement as the following:

$$u = \frac{0.654\, bW\sigma l}{E_s A} \tag{3.7}$$

The width and height of the lattice are expressed, which gives $W = l(\sqrt{3} + 3)$ and

$H = l(\sqrt{3} + 1)$ respectively, where $A = bt$ is the cross-section of each bar, then could be used in Equation 3.7:

$$\varepsilon = \frac{u}{H} = \frac{0.654\, bW\sigma l}{E_s AH} = \frac{0.654\, bW\sigma l}{E_s btH} \tag{3.8}$$

Based on the elastic modulus definition, the value of Young's modulus is given as follows:

$$E = \frac{E_s t}{1.132\, l} \tag{3.9}$$

Therefore an analogous result is obtained for the in-plane stiffness of the lattice under axial loading:

$$\frac{E}{E_s} \approx 0.3173\, \bar{\rho} \tag{3.10}$$

In contrast to the in-plane elastic modulus property shown in Table 2.2 for other known lattice cells, the result obtained above shows that the SST lattice is not stiff enough compared to other lattice topologies, including the kagome, triangular, mixed and square lattices, because the value of the stiffness coefficient B is lower for the SST lattice, but it is also very close to other lattice topologies.

3.3 Compressive Strength

The strength of a lattice cell is defined as the amount of stress that the structure can withstand before elastic yielding or elastic bucking occurs. In this section, both the value of elastic buckling strength and the value of plastic yielding strength under uniaxial compressive loading are investigated. , It is assumed that when the SST lattice is subjected to uniaxial compressive loading the structure experiences stress buckling at a very low relative density values, including $0.001, 0.003, 0.01$ and 0.03. In contrast, the SST lattice structure undergoes stress yield at high relative densities, including $0.08, 0.1, 0.15$ and 0.2. The combination of these results can help us to understand the nature of the failure mode. Therefore, it is assumed that the elastic buckling mode in the SST lattice is changed to a plastic yielding mode at the critical point of relative density under the axial compression loading mechanism.

The buckling strength of the lattice is defined along with the elastic buckling strength of the beam. For elastic buckling, we must equate the Euler buckling load with the force in the most loaded bar in this case this would be T_1according to Table 3.1, the buckling strength is defined as the following:

$$T_1 = \frac{n^2 \pi^2 E_s I}{(l)^2} \tag{3.11}$$

The parameter n is known as the end constraint factor, which is based on the degree of restriction of rotation at the ends.

EI is the bending stiffness of the bars. When rotation is built in at one end and freely allowed at the other end, $n = 0.5$; when rotation is restrained as in the case of fixed ends, $n = 2$ (Fan et al. 2009, Gibson and Ashby, 2010) Symbol l denotes the edge length of the bars between the nodes. For a cell wall of a lattice loaded by axial force, the load on the wall from adjacent joints lies between these limits, so $0.5 < n < 2$ (Fan et al. 2009). T_1 is the most loaded beam in the cell wall and W is the width of the unit cell.

The elastic buckling strength of the lattice under uniaxial Compression is expressed as the following:

$$\frac{\sigma_{el}}{E_s} = 0.0322\, \bar{\rho}^3 n^2 \tag{3.12}$$

The study of the analytical modelling can be simplified by using the factor $n = 2$, which indicates that the joints are completely rigid and use fixed–fixed ends in the system. If the constant $n = 2$ for the system:

$$\frac{\sigma_{el}}{E_s} = 0.1288\, \bar{\rho}^3 \tag{3.13}$$

The plastic yield strength of the lattice could be obtained by multiplying the yield strength by the cross sectional area. Hence the ratio of the stress to the yield strength of the SST lattice is given as follows:

$$\frac{\sigma}{\sigma_{ys}} = 0.3036\bar{\rho} \tag{3.14}$$

According to Table 2.2 the elastic buckling strength (C buckling strength coefficient) of the SST lattice under uniaxial compressive loading is slightly stronger than square cell and much stronger than mixed and triangular lattices. Also, the SST lattice is much weaker than kagome lattice.

According to Table 2.2 the obtained value of the D coefficient (yield strength coefficient) for SST lattice depicts that in contrast with other stretching dominated cell topologies, the SST lattice is slightly a little weaker than triangular and mixed cells, as is much weaker than Square and kagome cell topologies.

The critical relative density of the collapse mode in the system can be determined using the values of the yield strength coefficient D, d and the buckling strength coefficient C, c in the following equation:

$$\bar{\rho}_{Critical} = \left(\frac{D}{C}\frac{\sigma_{ys}}{E_s}\right)^{\frac{1}{c-d}} \tag{3.15}$$

$$\bar{\rho}_{Critical} = 1.534\sqrt{\frac{\sigma_{ys}}{E_s}} \tag{3.16}$$

The critical relative density of the SST lattice directly is dependent on the stiffness property of the solid material as well as on the tensile strength. The SST lattice is considered as a perfect lattice to study the analytical modelling of its in-plane property under uniaxial loading. The result of the analytical modelling calculation in this chapter is verified by comparing the outcome obtained by the FEA method in chapter 5.

3.4 Effective Shear Modulus

The periodic SST lattice is subjected to shear loading in the x direction, as shown in Figure 3.3. There are 3 unknown forces acting on the bars, including T_1, T_2 and T_3 under shear loading condition. In order to calculate the value of these shear forces, the bars affected by the bending loading are neglected.

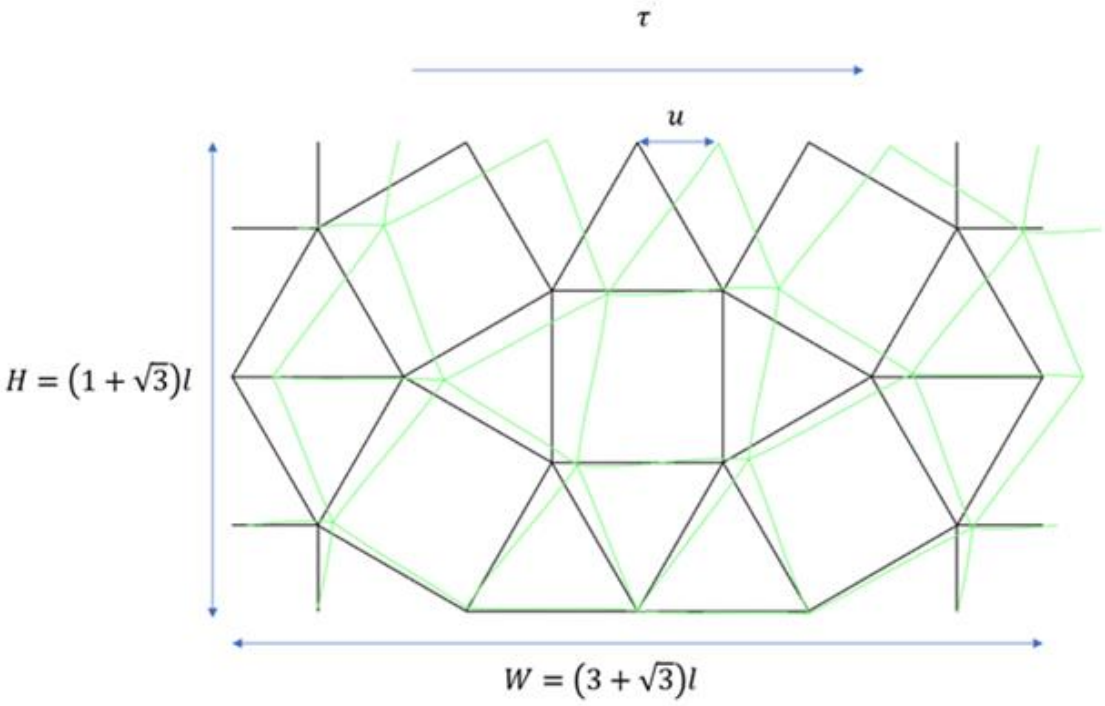

Figure 3.3: In shear loading case, there are three unknown forces acting on the bars T_1, T_2 and T_3. In order to calculate the value of forces, the bars affected by bending loading are neglected.

Considering aforementioned idea, 3 separate equations are required in order to solve the system. In Appendix 3, a series of calculations are performed to determine the value of 3 unknown shear forces T_1, T_2 and T_3 using a computational solver, as shown in Figure 2 in Appendix 3. The values of the shear forces for T_1, T_2 and T_3 are determined giving the results in Table 3.2.

$$\Sigma F_x = T_1 \cos 60° - T_2 \cos 30° - T_3 \cos 60° = 0 \tag{3.17}$$

$$\Sigma F_y = -T_1 \sin 60° + T_2 \sin 30° - T_3 \sin 60° = 0 \quad (3.18)$$

$$\Sigma F_x = -T_1 \cos 60° - T_2 \cos 30° + T_3 \cos 60° = \tau bW \quad (3.19)$$

Table 3.2: The values of shear forces applied in the system.

T1	$-0.6667\tau bW$	*Compression*
T2	$-0.5774\tau bW$	*Compression*
T3	$0.3333\tau bW$	*Tension*

The next stage for the analytical modelling study of the effective shear modulus of the SST lattice would be to determine the displacement of the top nodes in the unit cell. The displacement of the bare can be obtained either by using the trigonometric method to find $\delta_1$and δ_2 and then relating these results to the strain of the bars, or applying the principle of virtual work to find δ, neglecting the bars affected by bending mechanism in this analysis. In this study the principle of virtual work is used to calculate the value of shear displacement, which is described in more detail in Appendix 4.

Using the result obtained in the Table 4 in Appendix 4 and inserting these values into Equation 4.4 the shear displacement is obtained:

$$\tau bWu = \Sigma T_i \left(T_i \frac{l}{E_s A} \right) \quad (3.20)$$

$$u = \frac{1.7775\ lT}{E_s A} \quad (3.21)$$

Where $A = bt$ is the cross-section of each bar. By rearranging equations, we introduce a new formula as the following:

$$\gamma = \frac{u}{H} = \frac{1.7775\ l\tau W}{tE_s H} \quad (3.22)$$

Therefore an analogous result is obtained for the in-plane effective shear modulus of the lattice under shear stress:

$$\frac{G}{E_s} = 0.1166\ \bar{\rho} \quad (3.23)$$

The result obtained above, when compared with the in-plane effective shear modulus for other known cell walls as shown in Table 2.2, depicts that the SST lattice is stiffer than the square and mixed cell under the effect of shear stress. In contrast, the SST lattice is not stiff enough under shear loading as other lattice topologies, including the kagome and triangular lattices, because

the value of the shear modulus coefficient M is the lowest for the SST lattice, but is also very close to the kagome and triangular cell topologies.

3.5 Shear Strength

In this section, both the values of the elastic shear buckling and the plastic shear yielding are investigated under shear loading condition. It is predicted that when the SST lattice is subjected to a shear stress, the structure experiences the stress shear buckling at very low relative density values. In contrast, the structure of the lattice undergoes plastic yield stress at higher relative densities.

The shear buckling strength of the lattice is defined in relation to the elastic shear buckling strength of the beam. For the elastic shear buckling strength, we have to equate the Euler buckling load with the force in the most loaded bars, in this case this would be T_1according to Table 3.2, where the shear buckling strength is defined as the following:

$$T_1 = \frac{n^2\pi^2 E_s I}{(l)^2} = 0.3333\tau bW \tag{3.24}$$

The study of the analytical modelling can be simplified by using the factor $n = 2$, which indicates that the joints are completely rigid and use fixed–fixed ends in the system. If the constant $n = 2$ for the system:

$$\frac{\tau_{el}}{E_s} = 0.0483\ \bar{\rho}^3 \tag{3.25}$$

The plastic shear yield strength of the lattice could be obtained by multiplying the yield strength by cross-sectional area of the lattice:

$$0.3333\ \tau bW = \sigma_{ys} bt \tag{3.26}$$

Hence the plastic shear yield strength of the lattice is given as the following:

$$\frac{\tau}{\sigma_{ys}} = 0{,}2277\bar{\rho} \tag{3.27}$$

Unfortunately, no particular values have been reported for the elastic shear buckling strength, so it is difficult to compare the shear buckling strength value of the SST lattice with other known cell topologies.

According to Table 2.2, the obtained value of the shear yield strength coefficient S for the SST lattice in contrast with other stretching dominated cell topologies, is slightly a little stronger than the mixed cells and much stronger than the square lattice topology. However, it is much weaker than the triangular and kagome cell topologies.

4 Finite Element Analysis of the SST lattice

The study of the in-plan mechanical properties of the SST lattice is carried out in this chapter using the FEA method. The obtained results are used in order to verify the results of the analytical calculation in the Chapter 5. The commercial software Abaqus CAE is employed to perform the FEA simulations for the study of the elastic modulus, compressive strength, shear modulus and shear strength characteristics of the SST lattice.

4.1 $2D$ Geometry Definition and Meshing Process

As shown in Figure 4.1, during the FEA study, the unit cell of the SST lattice is considered as linear elastic -perfectly plastic solid, and the lattice structure is defined by several mechanical properties, including Poisson's ratio $v = 0.3$, modulus of elasticity $E_s = 200GPa$ and a yield strength $\sigma_{ys} = 200MPa$.

The meshing process of the lattice structure is implemented during the FEA study by 720 numbers of the $B21$ type beam elements using the global size of mesh 1 mm. These parameters are kept constant during all steps of the simulation process.

As shown in Figure 3.1, the length of each bar is fixed at 20 mm. The size of the unit cell designed in the simulation from FE is 94,641 mm × 54,641 mm.

Based on Equation 2.1, the relative density of the lattice depends on the length l and thickness t of the beam, so these parameters could be changed to alter the value of the relative density of the lattice at each simulation step. In this case, the length of the bar is kept constant while the thickness changes. The FE simulation steps are performed for the SST lattices with various values of the relative density $\bar{\rho}$ from 0.001 to 0.2.

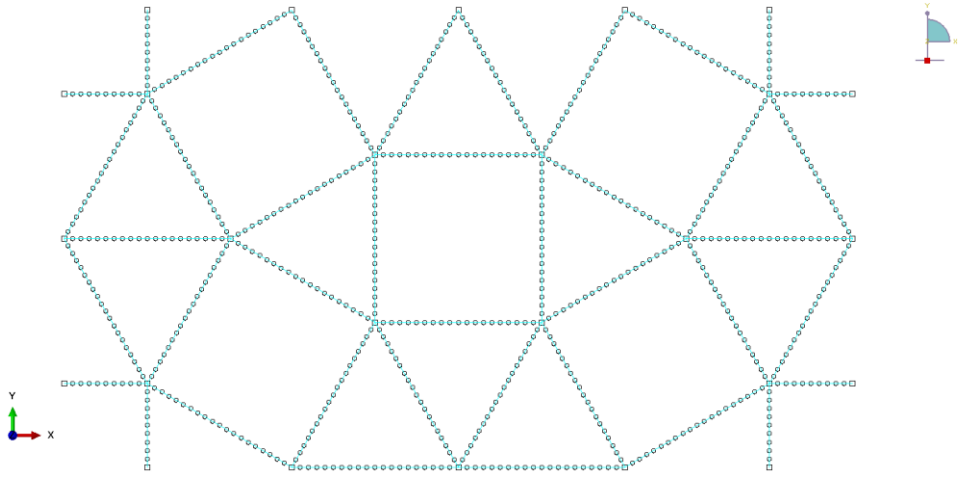

Figure 4.1: The meshing process of the SST lattice structure is conducted by *720* numbers of $B21$ type beam elements together with the global size of mesh 1 mm applied during the FEA study.

The desired topology of the SST lattice is designed in a $2D$ wireframe. The beam cross-section used for the lattice is defined by the thickness t and the out of plane depth for beam b. The values of the out of plane depth for the model remain constant at $b = 0.6$ for all relative densities, while the thickness of the beam t increases as the value of the relative density of the lattice is maximized for each FEA simulation.

4.2 Description of the FEA Model for Axial Loading Simulation

To maintain the periodicity of the SST lattice, a number of constraints are introduced between the nodes, as illustrated in Figure 4.2. Constraint equations are defined for all nodes located at the boundary around the lattice structure. If the unit cell is copied to create a larger lattice, node $1a$ is connected to node$1b$, and so on, as shown in Figure 4.2.

All constraints listed here are based on this general equation:

$$\Delta u_i = \varepsilon_{ij} \Delta x_j \tag{4.1}$$

The lattice is modelled in $2D$ with beam elements, each node has 3 degrees of freedom:

1. displacement along x.

2. displacement along y.

6. rotation around z.

The following notation $u_2^{[1a]}$ is used, which means the displacement along y (subscript 2) of node $1a$. The numbers $(1,2,6)$ correspond to the notation used in the commercial software Abaqus CAE. The first constraint is that the rotation around z should be the same for all corresponding nodes:

$$u_6^{[ia]} - u_6^{[ib]} = 0 \quad for\ i = 1,2,3,\dots,8 \tag{4.2}$$

To define the other constraints, we need to know the loading scenario. We can start by loading the lattice in compression in the y-direction, as shown in Figure 4.2.

The nodes on the left and right side must move vertically by the same amount. Therefore the constraints are as the following:

$$u_2^{[ia]} - u_2^{[ib]} = 0 \quad for\ i = 6,7,8 \tag{4.3}$$

The next step is more complicated. If the lattice expands in the vertical direction, it may shrink in the horizontal direction. However, each corresponding node must to shrink by the same amount.

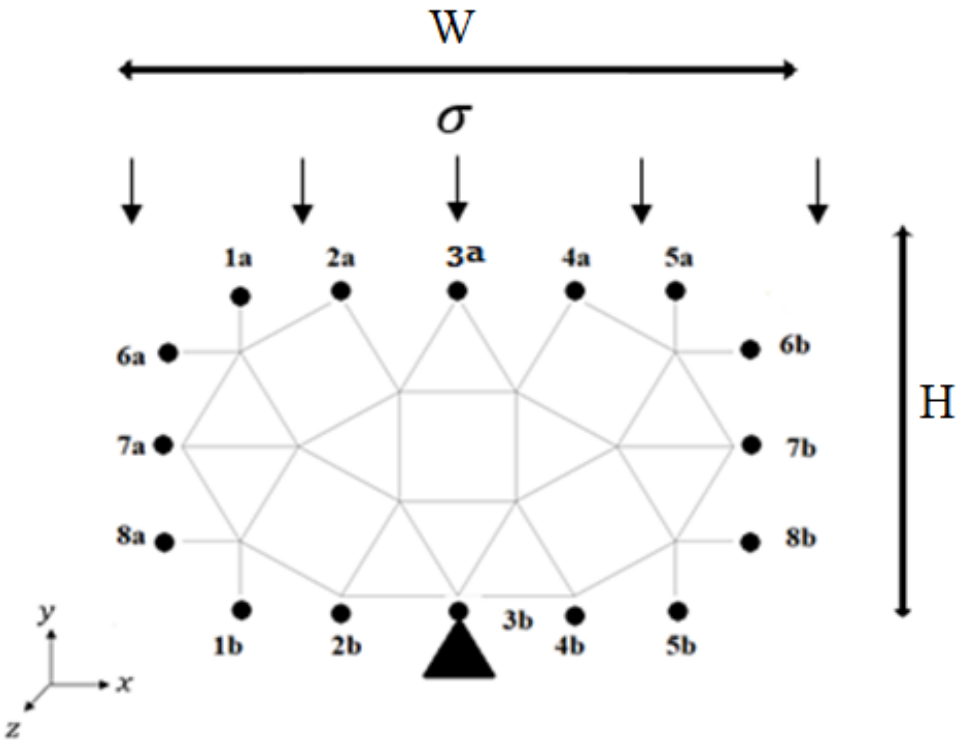

Figure 4.2: The prescribed displacement in the vertical direction at node $3a$.

Node 6 moves freely, and nodes 7 and 8 shrink by the same amount.

This constraint is as the following:

$$u_1^{[ia]} - u_1^{[ib]} - u_1^{[6a]} + u_1^{[6b]} = 0 \quad for\ i = 7,8 \tag{4.4}$$

Finally, we deal with the top and bottom side. To ensure that the nodes are connected, with each other the constraint is defined as the following:

$$u_1^{[ia]} - u_1^{[ib]} = 0 \quad for\ i = 1, \dots, 5 \tag{4.5}$$

In the vertical direction, we will set up the following equation:

$$u_2^{[ia]} - u_2^{[ib]} - u_2^{[3a]} + u_2^{[3b]} = 0 \quad for\ i = 1,2,4,5 \tag{4.6}$$

Finally, in the boundary conditions will be as follows:

- A pin joint at node 3b.
- A prescribed displacement in vertical direction at node $3b$. A boundary condition of Pinned type is applied at node $3a$ in the unit sell of the SST lattice, as shown in Figure 4.2.

4.3 Description of the FEA Model for Shear Loading Simulation

The constraint equations are applied around the boundary of the lattice model to perform the FEA study. For this purpose, node $1a$ is connected to node$1b$, and so on, as revealed in Figure 4.3. All constraints listed here are based on this general equation:

$$\Delta u_i = \gamma_{ij} \Delta x_j \tag{4.7}$$

Where $\varepsilon_{12} = \varepsilon_{21} = u/H$, and $\varepsilon_{11} = \varepsilon_{22} = 0$.

The lattice is modelled in $2D$ using beam elements, which means that each node has 3 degrees-of-freedom:

1: displacement along x.

2: displacement along y.

6: rotation about z.

The following notation $u_2^{[1a]}$ is used, which means the displacement along x (subscript2) of node $1a$.

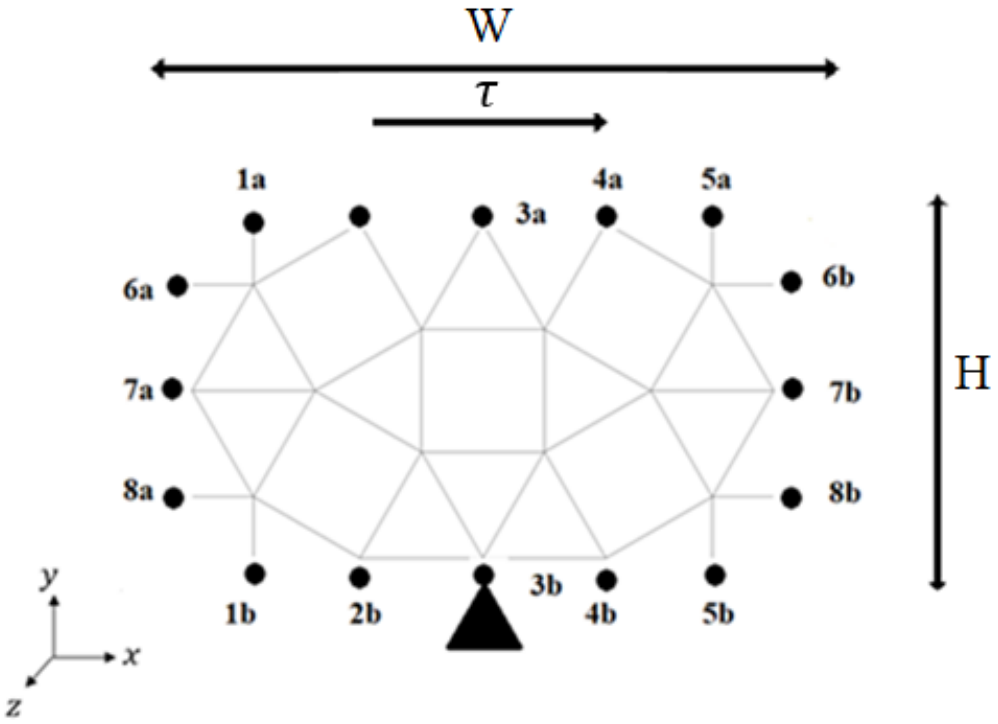

Figure 4.3:. The applied nodal constraint and boundary condition the lattice under shear force.

The numbers $(1,2,6)$ correspond to the notation used in Abaqus. The rotation around z should be the same for all corresponding nodes.

$$u_6^{[ia]} - u_6^{[ib]} = 0 \quad \text{for } i = 1, \dots, 8 \tag{4.8}$$

Boundary conditions could be implemented as the following:

- Nodes $3b$ is pinned, not for the parameters ux and $3y$ and
- prescribed displacement u in the horizontal direction is applied to node $3a$.

Considering Equation 4.7 and using to the top and bottom sides, which gives:

$$u_1^{[ia]} - u_1^{[ib]} = u_1^{[3a]} - u_1^{[3b]} \quad \text{for } i = 1,2,4,5 \tag{4.9}$$

$$u_2^{[ia]} - u_2^{[ib]} = 0 \quad \text{for } i = 1,2,3,4,5 \tag{4.10}$$

On the left and right sides surfaces:

$$u_1^{[ia]} - u_1^{[ib]} = 0 \quad \text{for } i = 6,7,8 \tag{4.11}$$

$$u_2^{[ia]} - u_2^{[ib]} = 0 \quad \text{for } i = 6,7,8 \tag{4.12}$$

$$u_1^{[ia]} - u_1^{[ib]} = u_1^{[3a]} - u_1^{[3b]} \quad \text{for } i = 1,2,4,5 \tag{4.13}$$

Indicating that we need 4 different equations as follows:

$$u_1^{[1a]} - u_1^{[1b]} - u_1^{[3a]} + u_1^{[3b]} = 0 \tag{4.14}$$

$$u_1^{[2a]} - u_1^{[2b]} - u_1^{[3a]} + u_1^{[3b]} = 0 \tag{4.15}$$

$$u_1^{[4a]} - u_1^{[4b]} - u_1^{[3a]} + u_1^{[3b]} = 0 \tag{4.16}$$

$$u_1^{[5a]} - u_1^{[5b]} - u_1^{[3a]} + u_1^{[3b]} = 0 \tag{4.17}$$

5 Results and Discussion

This chapter aims to compare the results determined with the two methods used in the previous chapters. This chapter of the thesis discusses the differences between the predicted results of the FEA technique with the analytical result, in cases of either axial or shear loading condition. The analytical result shows the mechanical properties of the perfect lattice, which are considered as an excellent criterion values. These mechanical properties of the SST have been validated and approved using the predicted FEA results.

5.1 Comparison of Elastic Modulus

The study in this chapter focuses on how the elastic modulus of the SST lattice varies as a function of relative density. For this purpose, all constraint equations are implemented, as explained in the previous section. As shown in Figure 4.2, node $3b$ is pinned and fixed, when node $3a$ moves upwards $\delta = 2$ using the prescribed displacement in direction y. The commercial Abaqus CAE software calculates the force corresponding to the prescribed displacement. The FEA simulation can be used to determine the force and displacement predictions. Using Equation 5.1, the results obtained for forces and displacements could be converted into a plot of stress versus strain, in which the slope shows the initial value of the stiffness of the lattice, as shown in Figure 5.2.

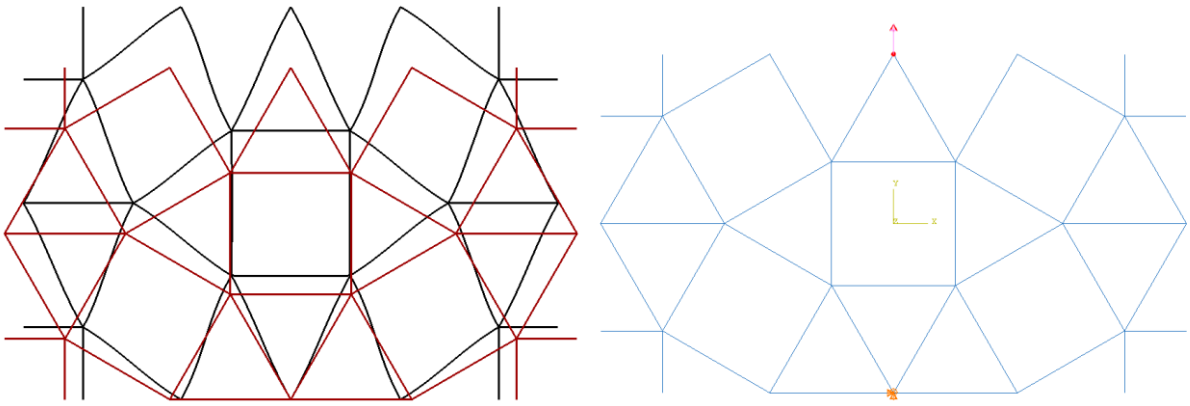

Figure 5.1: (Left) Deformed unit cell, shown in black colour under axial tension force and superimposed unit cell above the original unit cell. (Right) Applied axial tensile force at the upper node and applied boundary condition at the lower node of the unit cell.

The constraint equations are applied so that the unit cell experiences the uniaxial tensile forces. The bars are carrying axial forces, but not only axial forces, because they are modelled as beams so they can also experience a bending moment. This allows them to bend with the beam. In the analytical modelling study of the stiffness, we assume that all bars are only affected by axial

loads. However, in the FEA study there are a number of bars that are also affected by bending forces.

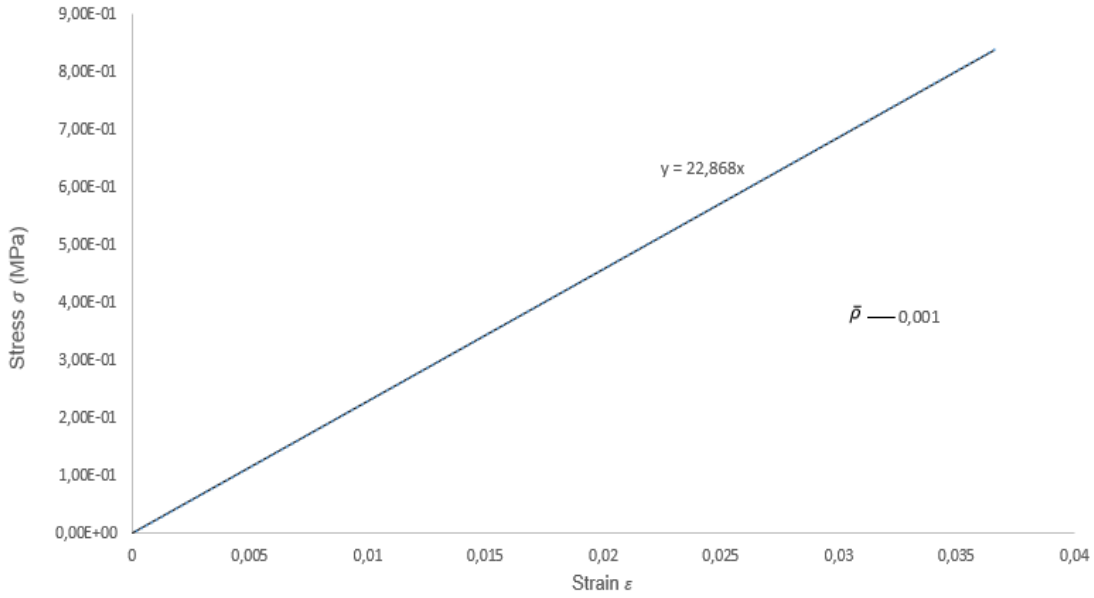

Figure 5.2: Stress-strain response of the SST unit cell and the initial value of the elastic modulus of the SST lattice at a relative density of 0.001.

In order to determine the value of the modulus of elasticity, the value of wall thickness can be calculated as the certain value of relative density at which the length of the bars remains constant. The obtained value of the wall thickness is inserted into the commercial software Abaqus CAE in order to calculate the value of the axial tensile force. During this simulation process, the lattice obeys the linear elastic mechanism. In addition, the value of the modulus of elasticity is determined based on Equation 5.1, where the stress is the nominal stress applied in the vertical direction of the lattice:

$$E = \frac{\sigma}{\varepsilon} = \frac{\frac{F}{bW}}{\frac{\delta}{H}} \tag{5.1}$$

These steps can be repeated for the other values of the relative density increments, including $0.001, 0.003, 0.01, 0.03, 0.08, 0.1, 0.15$ and 0.2. The result obtained for the stiffness can be normalized by the modulus of elasticity used in the material property as a function of the relative density.

Figure 5.4 shows the variable $S11$ stress for the relative densities of the lattice for 0.001 and 0.2 respectively. The bars primarily carry axial stresses and are loaded either in compression or in tension. The result seems to be fine and reasonable, as the bars are deformed symmetrically.

The pictures in Figure 5.4 illustrate that at low relative densities, the bars are not very strongly affected by the bending moment, because the bars experience much more elastic buckling due to their nature of slenderness. Nevertheless, bending moments increase at higher relative densities, because there is a plastic yielding mechanism as the main deformation mode, which causes an increase in resistance to the bending effect. However, this type of deformation mechanism and the bar bending do not result in the SST lattice becoming a bending dominated structure. It can therefore be concluded that the SST lattice is stretching dominated cell topology when its structure experiences an axial stress along x and y directions.

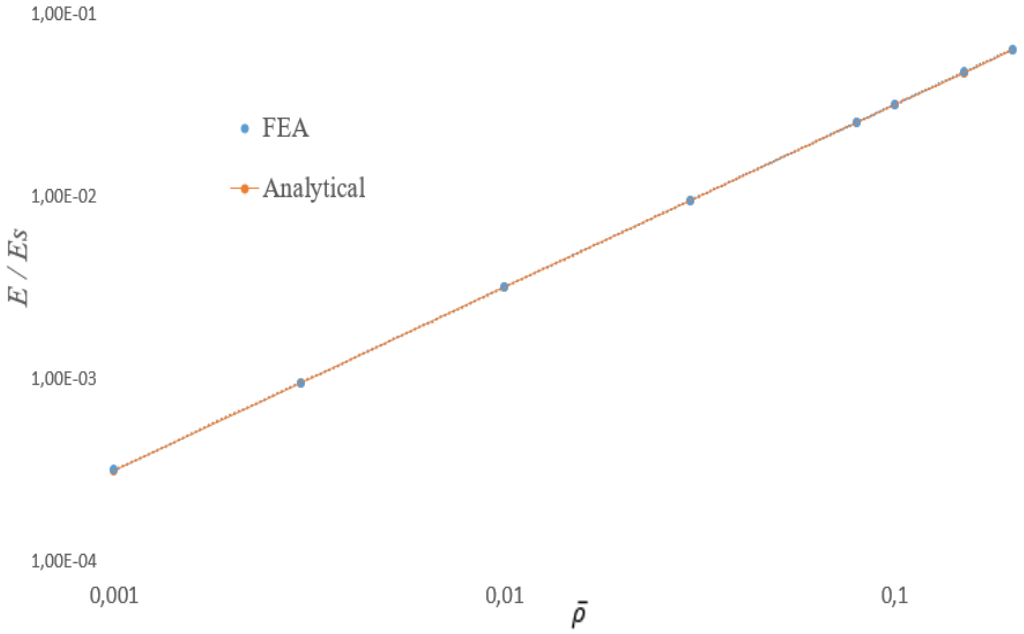

Figure 5.3: Normalized elastic modulus as a function of relative densities for the SST lattice. FEA and analytical results are in good agreement.

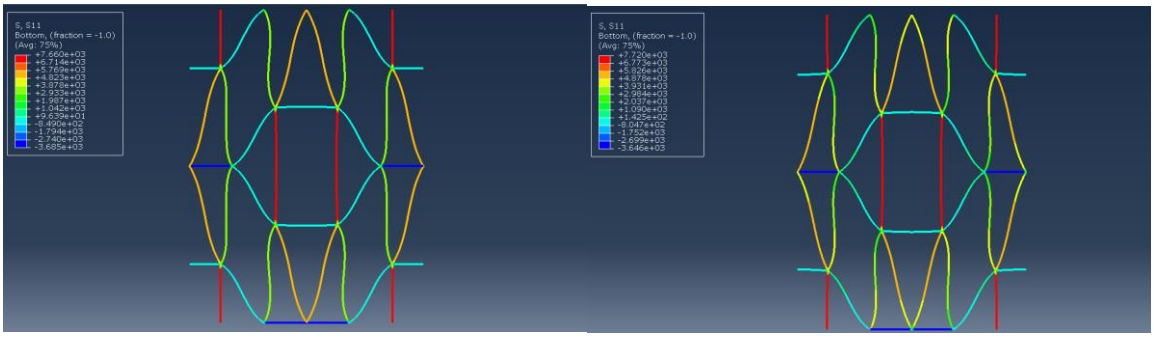

(a) (b)

Figure 5.4: Distribution of the variable S11 stress (MPa) in the lattice for the scenario of axial tensile load and the corresponding linear elastic regime for the relative densities of (a) 0.001 and (b) 0.2.

Figure 5.3 depicts the variation of the normalized elastic modulus as a function of relative densities when the SST lattice is subjected to an axial tensile load. The value of the stiffness

coefficient B indicates that the structure of the lattice is influenced by the stretching dominated mechanism under tensile force. The two results show that they are in good agreement. Figure 5.3 is underlining that the value of the stiffness obtained with the FEA method is slightly higher than that achieved with analytical modelling. This is because the coefficient of stiffness B and b for the FEA simulation is higher and also the slope of the line is slightly steeper compared to the analytical result. The outcome predicted by the FEA is somewhat stiffer by 0.5 % difference, which is due to the application of the nodal constraint around the model. We therefore conclude that the analytical results can be used as an excellent criterion for determining the stiffness of the SST lattice. We can conclude that both techniques are practicable for estimating the modulus of elasticity of the SST lattice.

5.2 Comparison of Compressive Strength

In this section the in-plane compressive strength of the lattice is predicted as a function of the relative density from 0.001 to 0.2. The linear-elastic mechanism was used in the previous section to study the stiffness property of the SST lattice, which needs to be modified by adding a plasticity parameter to the material section, including the yield strength σ_y 200 MPa and the plastic strain ε is 0. The material is linear-elastic and perfectly plastic.

When the lattice is loaded with the axial compression in the vertical direction, its strength is dictated by buckling in the bars, so that in the FEA study to capture the buckling, the option of nonlinear geometry can be considered. During the FEA study of the uniaxial compression property, we will consider the elastic regime when the bars are buckled. The same structure, nodal equations and boundary condition are applied as in the previous chapter. However, the displacement can be changed from tensile to compressive strength so the value of the displacement is altered to a negative value and the displacement acts downward in the y direction. The prediction for the plot of the normalized strength as a function of the relative density will be a line with two various slopes based on its failure mode. These failure modes shift at the critical density point $\bar{\rho}_{crit}$. To calculate the value of normalized strength, the nominal stress is calculated by the following Equation 5.2:

$$\sigma = \frac{F}{bW} \tag{5.2}$$

Where W is the width of the unit cell, b is the out of plane depth of the beam and F is the highest value of the force acting on the top edge of the unit cell. With the increasing thickness of the bar, the value of the relative density increases, which affects on the deformation mechanism of the lattice structure. It is predicted that the lattice structure maintains the forces at a very low relative density until the elastic buckling load is approached. However, after the point of critical relative density, the deformation mode shifts to the plastic yielding mode.

The picture in Figure 5.6 shows that the results obtained results seem to be reasonable. This is because the unit cell has two planes of symmetry and the loading distribution is uniform for the whole unit cell.

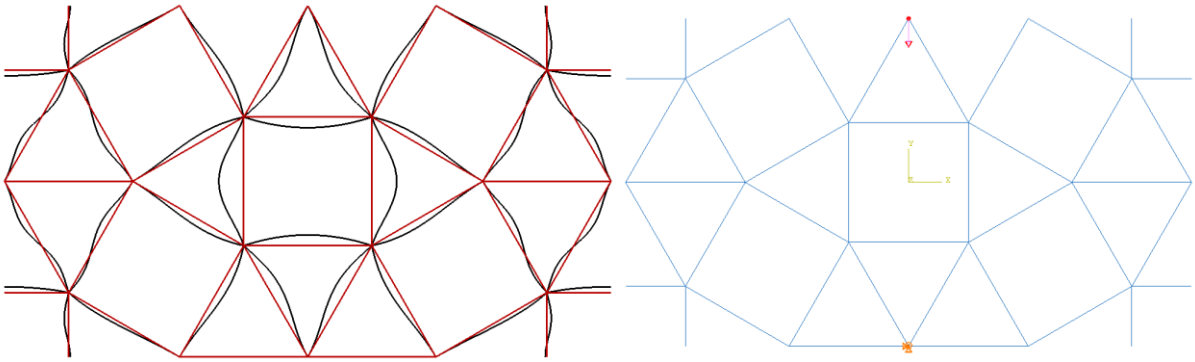

Figure 5.5: (Left) Deformed unit cell, shown in black colour under axial compressive force and superimposed unit cell above the original unit cell. (Right) Applied axial compressive force at the upper node and applied boundary condition at the lower node of the unit cell.

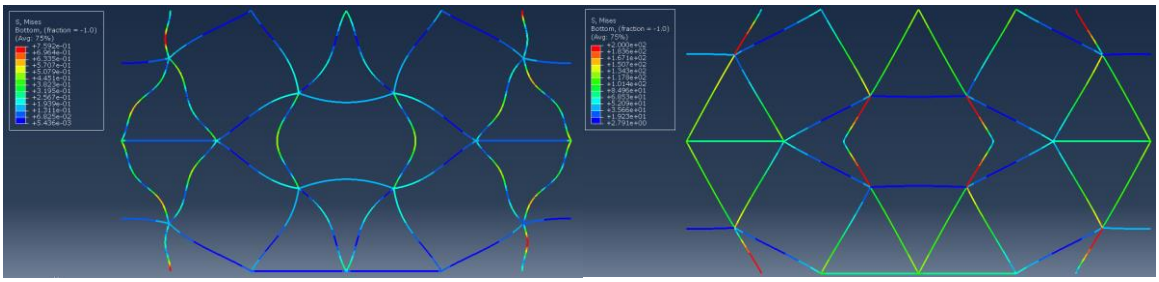

(a) (b)

Figure 5.6: Distribution of the von-Mises stress (MPa) in the SST lattice for the scenario of the axial compression loading for the relative densities for various relative densities of (a) 0.001, (b) 0.2.

The predicted FEA results confirm the fact that at the very low relative densities, including $0.001, 0.003, 0.01$ and , 0.03 under compressive axial loading, the lattice becoming the bending dominated and influenced by the elastic buckling mode. On the other hand, the SST lattice material shifts to the stretching dominated and affected by the plastic yielding mode under compressive axial loading at the high relative densities, including , $0.08, 0.1, 0.15$ and 0.2. At low values of relative density, the bars are very slender $t << l$. When the lattice is compressed, the bars buckle elastically if the axial force on the bar is equal to the Euler buckling load. (The axial stress in the bar is lower than the yield strength of the material). For these geometries the strength is scaled as $p3$. At higher values of relative density, the bars are chunkier. When the lattice is compressed, the axial stress in the bar reaches the yield strength of the material before buckling. This is plastic buckling. For these geometries, the strength is scaled as $p1$.

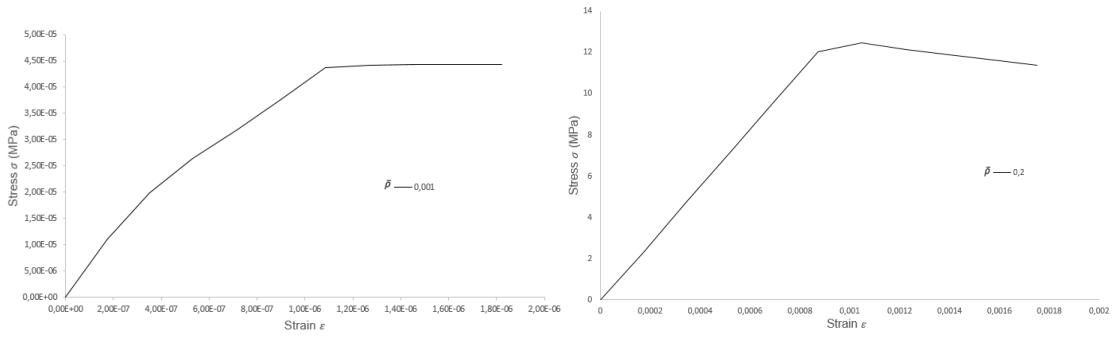

(a) (b)

Figure 5.7: Stress-strain response of the SST lattice under compressive load for various relative densities of (a) 0.001, (b) 0.2. The relative densities $0.001, 0{,}003, 0.01$ and 0.03 undergo elastic buckling while $0.08, 0.1, 0.15$ and 0.2 are influenced by plastic yielding.

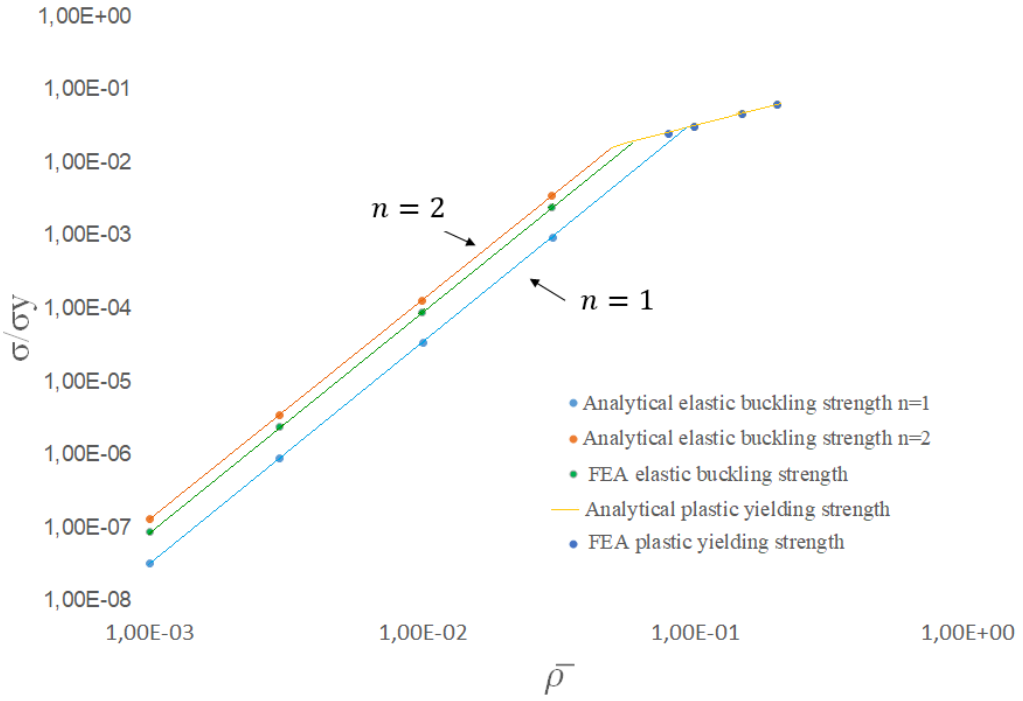

Figure 5.8: Normalized axial compressive strength as a function of relative densities for SST lattice. FEA and analytical results are in good agreement. The lattice is buckled elastically at low relative densities and deformed under plastic yielding mechanism at high densities.

Figure 5.8 demonstrated the comparison plot of the normalized strength of the lattice under axial compressive loading condition. The lattice is deformed under elastic buckling at low relative densities. Nevertheless, after exceeding the point of critical relative density, the deformation mode of the lattice is shifted to plastic yielding at high relative densities.

In the region of elastic buckling strength we can note the fact that the FEA result is weaker by $30\ \%$ than the analytical result because end constraint factor is used as $n = 2$ in the calculation, which indicates that the joints in the lattice are completely rigid. The SST lattice has a bending dominated feature in the region of elastic buckling strength because the bars are very slender and the axial forces on the bears are equal to the Euler buckling load.

On the contrary, the results of both methods are found to be in good agreement in the region of plastic yielding strength and the difference is only $1.1\ \%$. The SST lattice is dictated by a stretching dominated mechanism, because the bars are chunkier and the axial stress in the bar reaches the yield strength of the material.

5.3 Comparison of Effective Shear Modulus

This chapter investigates the shear modulus of the lattice as a function of the relative density. All the constraint equations are implemented as is described in the previous chapter. As Figure 4.3 shows, when node $3b$ is pinned and fixed, node $3a$ moves to direction of x, using the prescribed displacement $\delta = 2$. In the FEA simulation, the values of force and displacement are determined for each corresponding relative density. The bars are loaded with both shear load and bending moment and are modelled as beams. The obtained values in the previous section are used in the commercial software Abaqus CAE to determine the values of the shear forces at which the periodic cell wall satisfies the linear elastic mechanism. Thus the shear modulus of the lattice is calculated based on Equation 5.3:

$$G = \frac{\tau}{\gamma} = \frac{\frac{F}{bW}}{\frac{\Delta}{H}} \tag{5.3}$$

Using Equation 5.3, the results obtained for forces and displacements could be converted into a plot of stress versus strain, in which the slope shows the initial value of the elastic modulus of the SST lattice, as shown in Figure 5.9.

Figure 5.11 reveals the distribution of the $S11$ stress for the relative densities of the lattice. The bars are primarily affected by shear stresses. The bars in the lattice are uniformly loaded and the unit cell has two plans of symmetry, which depicts that the results obtained are reasonable. The bars are experienced elastic buckling at very low relative densities as well as very less bending moment.

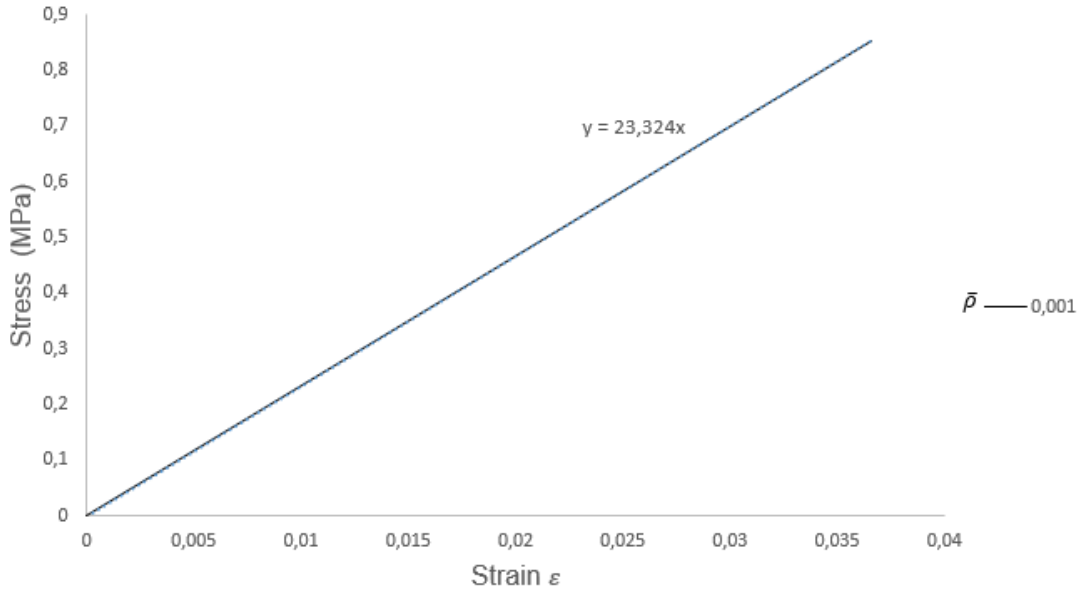

Figure 5.9: Stress-strain response of the SST unit cell and the initial value of the effective shear modulus of the SST lattice at a relative density of 0.001.

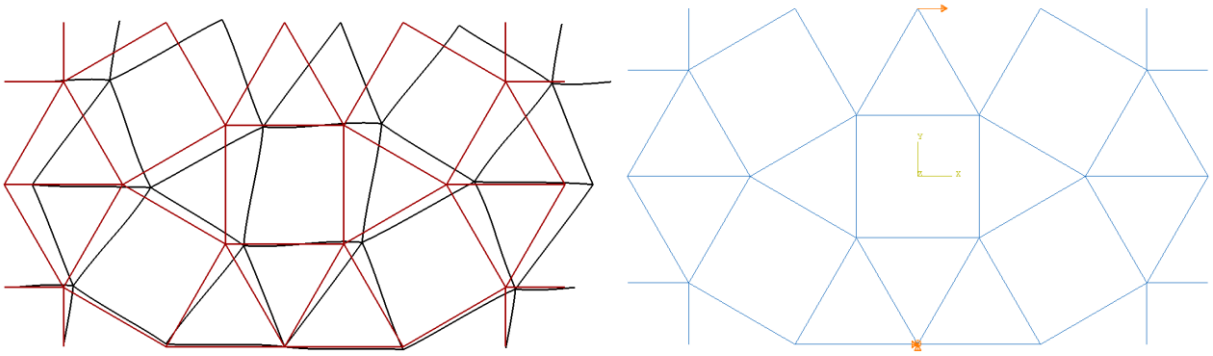

Figure 5.10: (Left) Deformed unit cell, shown in black colour under shear force and superimposed unit cell above the original unit cell. (Right) Applied shear force at the upper node and applied boundary condition at the lower node of the unit cell.

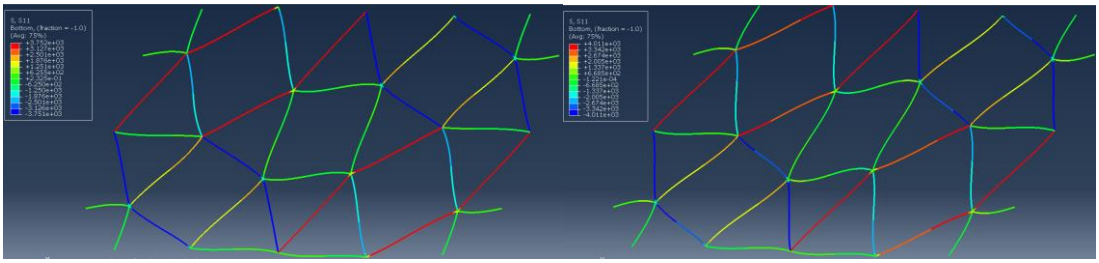

(a) (b)

Figure 5.11: Distribution of the variable S11 stress (MPa) in the lattice for the scenario of shear load and the corresponding linear elastic regime for various relative densities of (a) 0.001, (b) 0.2.

However, the bars are affected much more by bending moment due to to presence of plastic yielding mechanism as the main deformation mode at high relative densities. Despite that the experience of the bars under bending moment does not cause the lattice to become a bending dominated periodic cell wall. As a conclusion, we can define the SST lattice is a stretching dominated lattice structure under shear load. Figure 5.11 reveals that the presence of bending deformations under shear stress on the bars is maximized by increasing the bar thickness.

The aforementioned step could be used for other relative density increments from 0.001 to 0.2. The result obtained for the shear modulus could be divided by the elastic modulus of the solid, which is a dimensionless parameter. A plot could be drawn as normalized shear modulus as a function of relative density for the SST lattice, as shown in Figure 5.12.

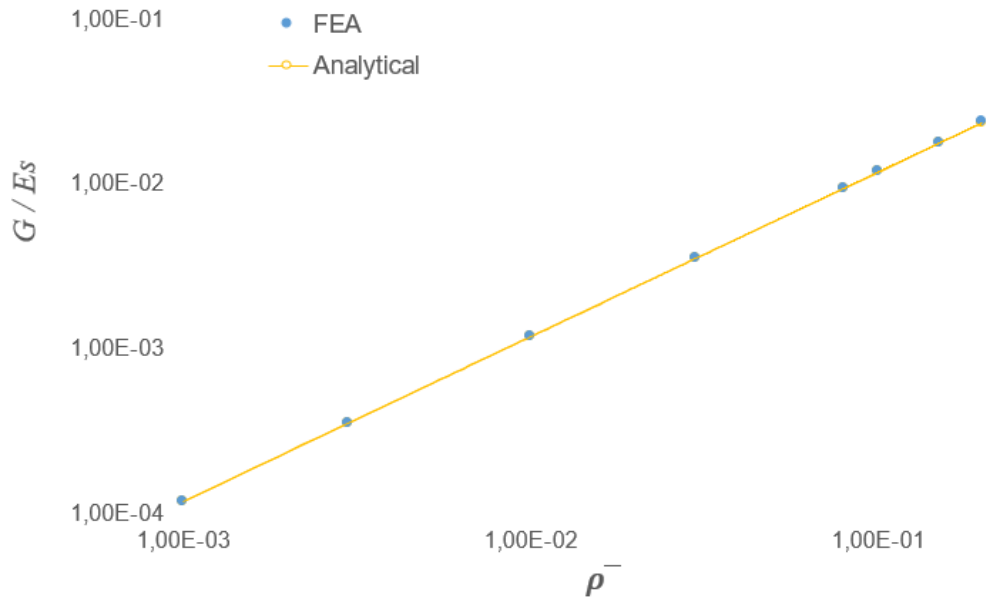

Figure 5.12: Normalized elastic modulus as a function of relative densities for the SST lattice. FEA and analytical results are in good agreement.

Figure 5.12 presents the change in shear modulus as a function of the relative density values when the SST lattice is subjected to shear stress. The plot shows that the value of the shear modulus obtained with the FEA method is slightly higher by 0.5 % difference than with analytical modelling. Because the stiffness coefficient M for the FEA simulation is higher and also the slope of the line is slightly steeper compared to the analytical result. The structure of the lattice exhibits the stretching dominated feature under shear stress. Overall, these results are closely matched and show good agreement, indicating that both techniques can be used to analysis the in-plane mechanical properties of the SST lattice.

5.4 Comparison of Shear Strength

In this chapter, the in-plane shear strength of the SST lattice is investigated as a function of the relative density from 0.001 to 0.2. The $2D$ model is modified by adding to the material section a plasticity property as yield strength σ_y 200 MPa and the plastic strain ε is equal to 0. It is therefore assumed that the lattice experiences a linear elastic and perfectly plastic mechanism. The lattice is subjected to a pure shear load in the x direction. The strength of the bars is dictated with elastic buckling mechanism, so we have to consider the option of nonlinear geometry during the FEA simulation to capture the elastic buckling. The similar set up with the same nodal equations is used as in the previous chapter. The implementation of the FEA study depends on the calculation of the nominal shear stress, which is determined as follows:

$$\tau = \frac{F}{bW} \tag{4.4}$$

Where W is the width of the unit cell, b is the out of plan depth of the beam and F is the highest value of the force acting on the top edge of the unit cell.

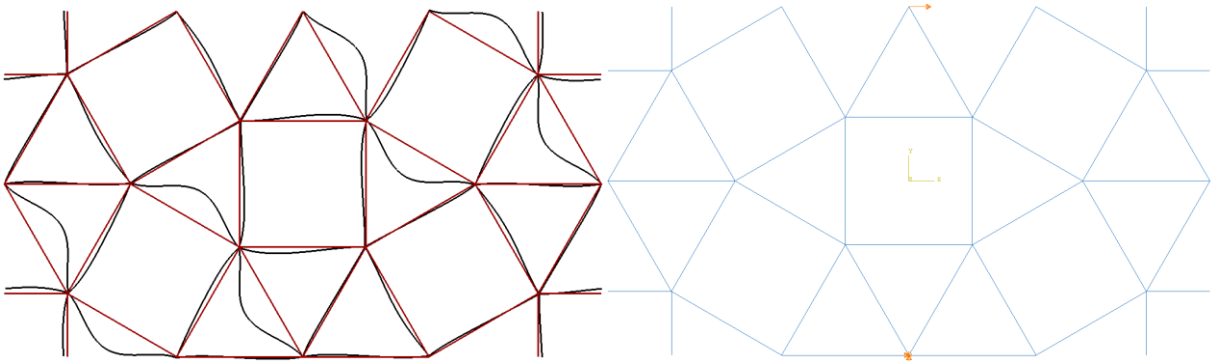

Figure 5.13: (Left) Deformed unit cell, shown in black colour under shear force and superimposed unit cell above the original unit cell. (Right) Applied shear force at the upper node and applied boundary condition at the lower node of the unit cell.

Figure 5.15 shows that the results of the FEA appear to be reasonable and satisfactory, since the force distribution in the unit cell is uniform and the unit cell has two planes of symmetry. It could be observed that the SST cell maintains forces up to the elastic shear buckling mode at very low densities and is bending dominated lattice. While after exceeding the critical density point, the deformation mechanism shifts to the plastic shear buckling mode and became stretching dominated lattice.

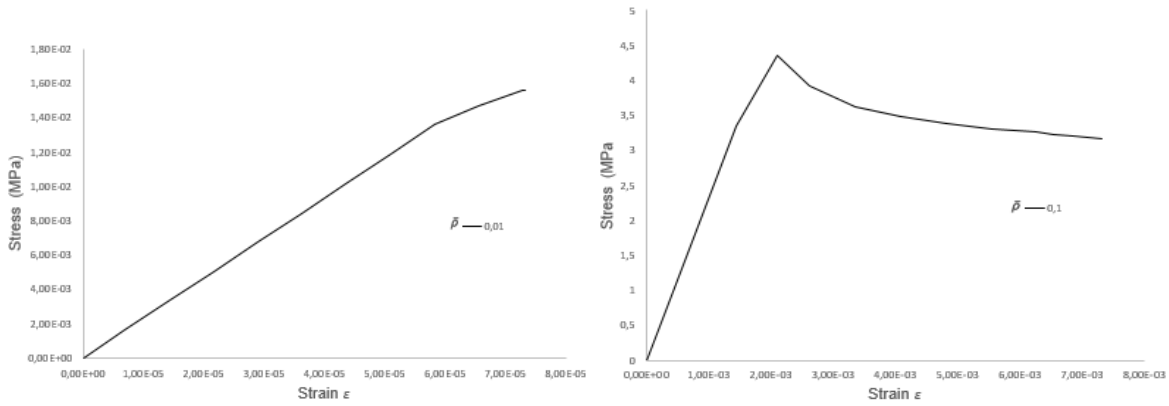

(a) (b)

Figure 5.14: Stress-strain response of the SST lattice under shear load for various relative densities of (a) 0.01, (b) 0.1. The relative densities $0.001, 0{,}003, 0.01$ and 0.03 undergo elastic buckling while $0.08, 0.1, 0.15$ and 0.2 are influenced by plastic yielding.

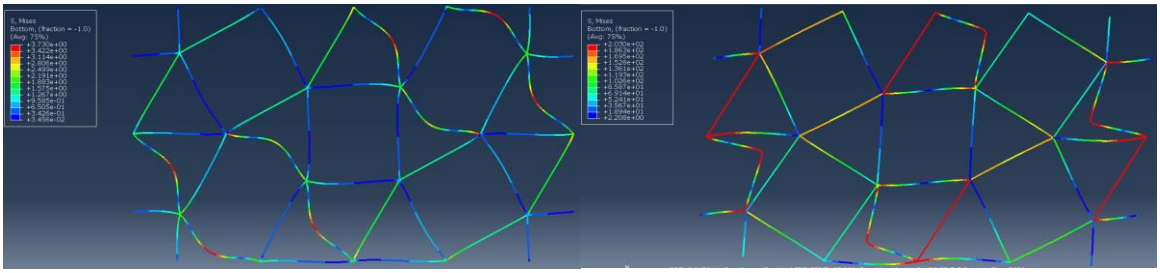

(a) (b)

Figure 5.15: Distribution of the von-Mises stress (MPa) in the SST lattice for the scenario of the shear loading for the relative densities of (a) 0.003 and (b) 0.1.

The shear strength of the SST lattice is plotted in Figure 5.16 as a function of the relative density. Figure 5.16 shows that in the region of elastic buckling strength, it can be concluded that the FEA result is 31.4 % difference stronger than the analytical result because its elastic shear buckling coefficient N is higher. This is due to the use of constrained nodes around the SST lattice.

On the contrary, the results of both methods are very similar in the plastic buckling region and the difference is only 6.1%. Because their plastic shear strength coefficient S is approximately the same.

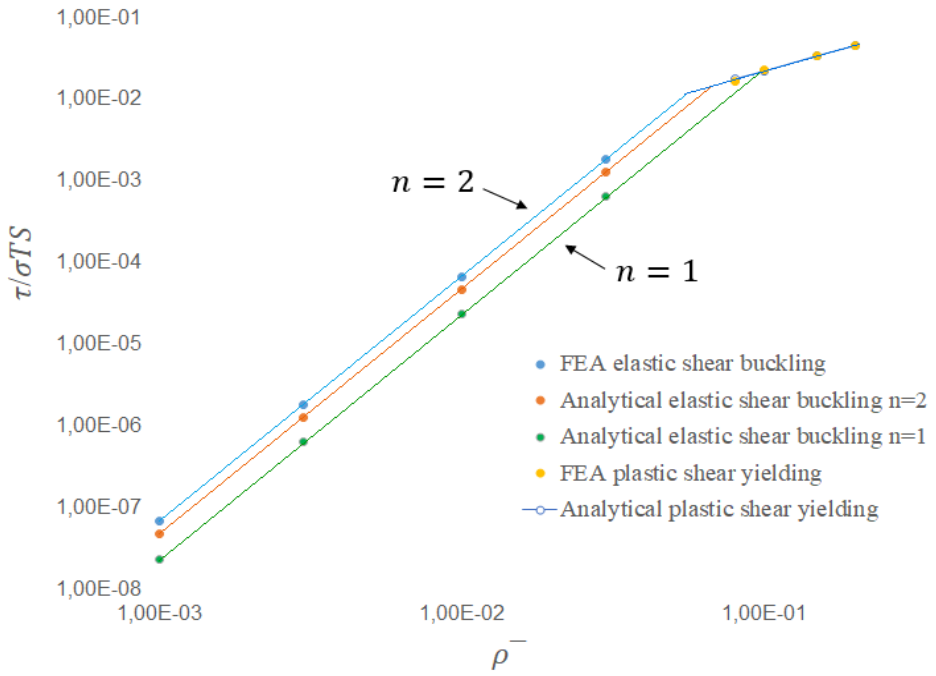

Figure 5.16: Comparison plot of the shear strength of the SST lattice in FEA and analytical techniques as a function of relative densities.

Table 5.1: Mechanical properties of the SST lattice in cases of shear and axial stresses. Comparison of the results obtained by FEA and analytical methods.

Methods	*Stiffness Coefficient B*	*Elastic buckling Compressive strength Coefficient C*	*Plastic yielding compressive strength Coefficient D*	*Shear modulus Coefficient M*	*Elastic buckling shear strength Coefficient N*	*Plastic yielding Compressive strength Coefficient S*
Analytical Modelling	*0.3171*	*0.1288*	*0.3036*	*0.1166*	*0.070*	*0.228*
FEA Technique	*0.3186*	*0.08979*	*0.307*	*0.1172*	*0.048*	*0.242*
Error difference	*0.5 %*	*30 %*	*1.1 %*	*0.5 %*	*31.4 %*	*6.1 %*

Methods	*Stiffness Coefficient b*	*Elastic buckling Compressive strength Coefficient c*	*Plastic yielding compressive strength Coefficient d*	*Shear modulus Coefficient m*	*Elastic buckling shear strength Coefficient n*	*Plastic yielding Compressive strength Coefficient s*
Analytical Modelling	*1*	*3*	*1*	*1*	*3*	*1*
FEA Technique	*1.0006*	*3.0023*	*1.059*	*1.0009*	*3.0021*	*1.024*
Error difference	*0.06 %*	*0.08 %*	*5.9 %*	*0.09 %*	*0.67 %*	*2.4 %*

5.5 Comparison with Other Stretching Dominated Lattice

This chapter aims to highlight the in-plane mechanical properties of SST and other stretching dominated periodic lattice cells under shear and axial loading conditions. Six different periodic lattice cells are reviewed in this study in order to investigate their in-plane properties such as stiffness, compressive strength, shear modulus and shear strength based on truss theory and simple beam theory. These results have already analytically been determined, so they need to be compared with the analytical outcome of the SST lattice from chapter 3. These mechanical properties are listed in Table 5.2.

Table 5.2: Coefficient of the in-plane mechanical properties of the other stretching dominated lattices and the SST lattice.

Lattice Geometry	*A*	*B*	*b*	*C*	*c*	*D*	*d*	*M*	*m*	*S*	*S*	*v*
Kagome Cell	$\sqrt{3}\,\frac{t}{l}$	0.333	1	0.366	3	0.5	1	0.125	1	0.289	1	0.33
Triangular Cell	$2\sqrt{3}\,\frac{t}{l}$	0.333	1	0.0914	3	0.333	1	0.125	1	0.289	1	0.33
Mixed Cell	$2+\sqrt{2}\,\frac{t}{l}$	0.369	1	0.029	3	0.369	1	0.104	1	0.207	1	0.146
Square Cell	$2\,\frac{t}{l}$	0.5	1	0.103	3	0.5	1	0.063	3	0.125	2	0.5 vr
SST Cell	$2.7846\,\frac{t}{l}$	0.3173	1	0.1288	3	0.3036	1	0.117	1	0.228	1	0.3

The value of the relative density constant A is reviewed between these lattices in Table 5.1. The results show that for a given value of t/l, the relative density of SST lattice is relatively lower than for the mixed and triangular lattices, so we can conclude that the SST periodic lattice is much lighter than the mixed and triangular . In contrast, for a given value of t/l the SST lattice is heavier than the kagome and square cell topology.

The in-plane stiffness property of other stretching dominated lattices and the SST cell are shown in Figure 5.5. The plot shows the variation of the normalized elastic modulus as a function of the relative densities from $0{,}001$ to 0.2. A line fitting between 8 points is drawn and the slope of this plot indicates the value of the modulus of elasticity coefficient B. The plot shows that the line of stiffness property for the kagome and triangular lattices are in good agreement, indicating that both lattice topologies have the same elastic modulus. The square lattice cell has the highest stiffness value and is stiffer than others and the SST cell is found to be inferior to the others. In comparison, the stiffness of the SST lattice is slightly lower than than the kagome, triangular and mixed cell walls, but much lower than that of the square topologies. Therefore, the SST lattice is found to be inferior to those of the square, mixed, triangular and kagome lattices.

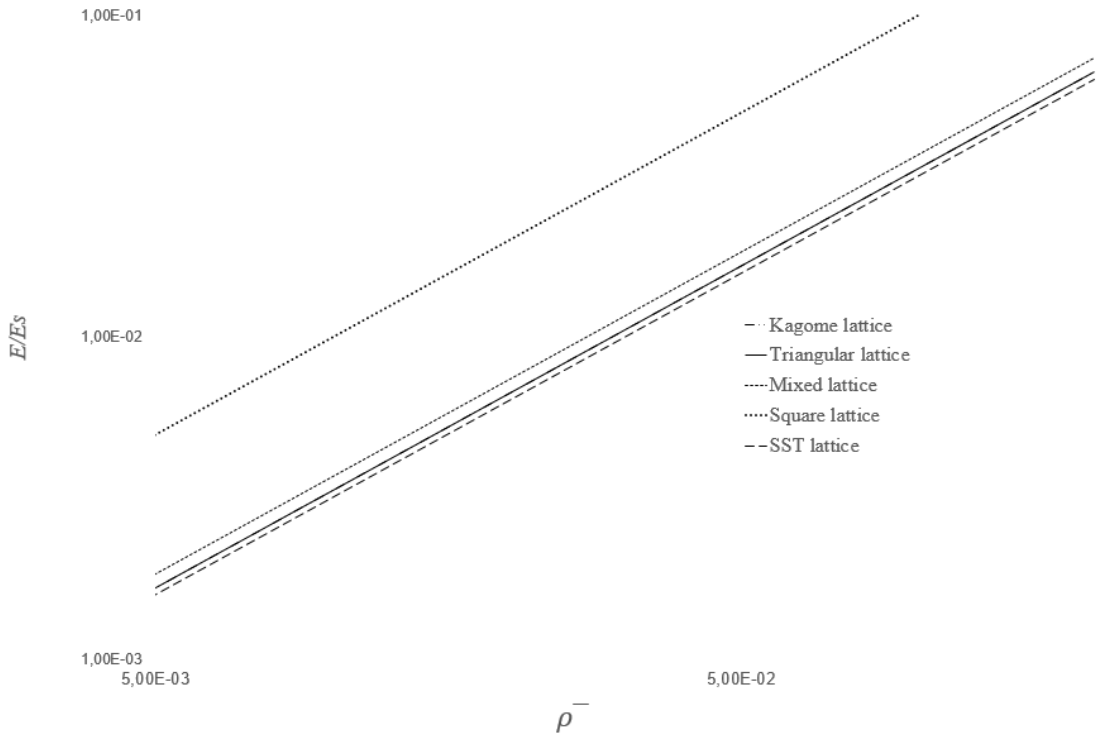

Figure 5.17: Comparative plot of the normalized stiffness as a function of relative density for SST and other stretching dominated lattices. The SST lattice is found to be inferior to those of the square, mixed, triangular and kagome lattices.

The normalized compressive strength property of other known lattices and the SST periodic cell are plotted as a function of the relative density, as shown in Figure 5.18 and 5.19, the two figures show two different slopes indicating the elastic buckling and plastic yielding modes respectively.

In the elastic buckling region, the mixed and triangular lattice topologies have the lowest buckling strength, while the kagome is the strongest. In terms of elastic strength, the SST lattice cell is slightly higher than square lattice and is found to be weaker than the kagome cell and with considerable amount stronger than the mixed and triangular lattice topologies.

In another region of the plot, where the plastic yielding mode of the lattice dominates, we can conclude that the kagome and square cell are superior to the others, in which both having the same yield strength properties. The SST lattice is found to be inferior to those of these lattices, although its yield strength property is slightly lower than the triangular and mixed lattices and their mechanical properties of yield strength closely matched to those of lattices under compressive axial stress.

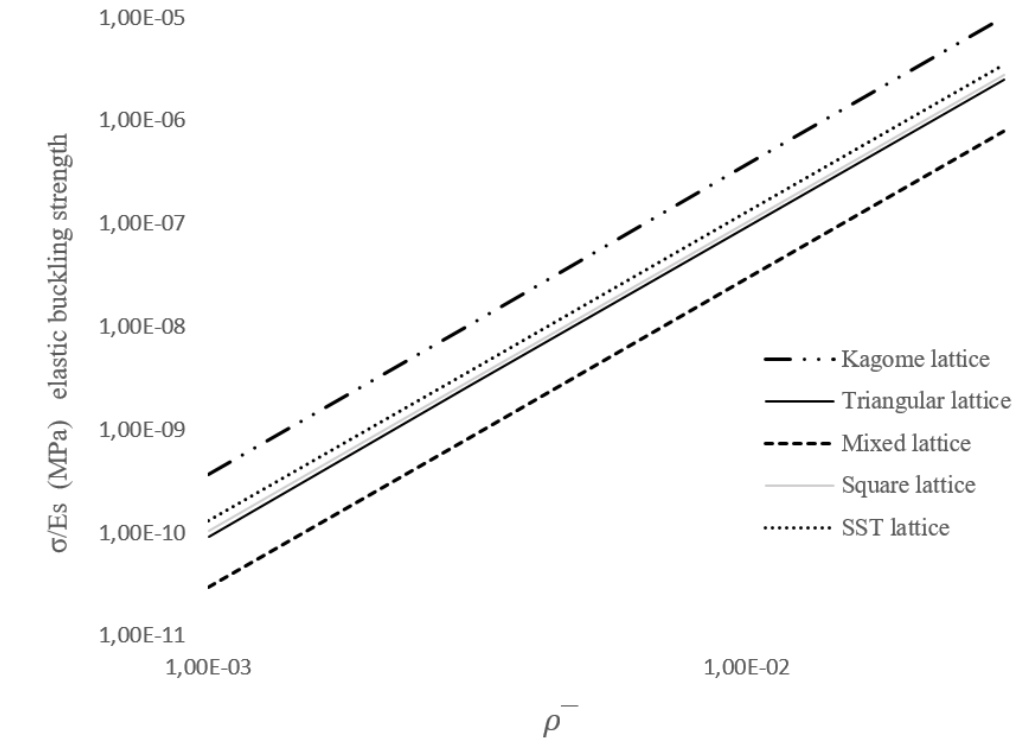

Figure 5.18: Comparative plot of the elastic buckling compressive strength as a function of relative density for SST and other stretching dominated lattices.

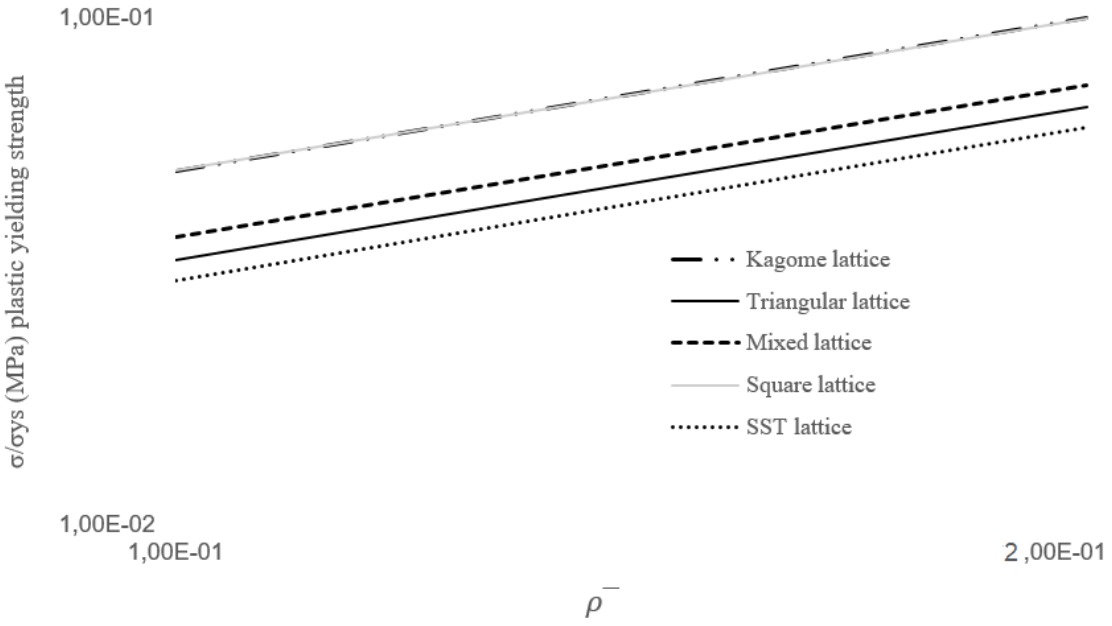

Figure 5.19: Comparative plot of the plastic yielding compressive strength as a function of relative density for SST and other stretching dominated lattices.

The in-plane effective shear modulus of other known lattices as well as the SST cell are shown in Figure 5.20. The plot illustrates the change in shear modulus as a function of the relative densities from 0,001 to 0.2. The result depicts that the shear modulus property lines for the kagome and triangular lattices are exactly in line with each other, signifying both lattice topologies have similar shear modulus properties under shear stress.

The kagome and triangular lattice cells have a higher shear modulus compared to others. On the other hand, the square lattice topology has the lowest shear modulus among the others. The square lattice has a different slope which indicates that it is a bending dominated lattice. In contrast, the SST lattice demonstrated an approximately similar shear modulus property as a function of relative densities for the triangular, mixed and kagome cell walls. This observation shows under shear stress, the SST shows a mechanical behaviour approximately similar to these lattices. More accurately, the shear modulus property of the SST lattice is slightly higher than for the mixed and a bit lower than the kagome and triangular periodic cells lattices.

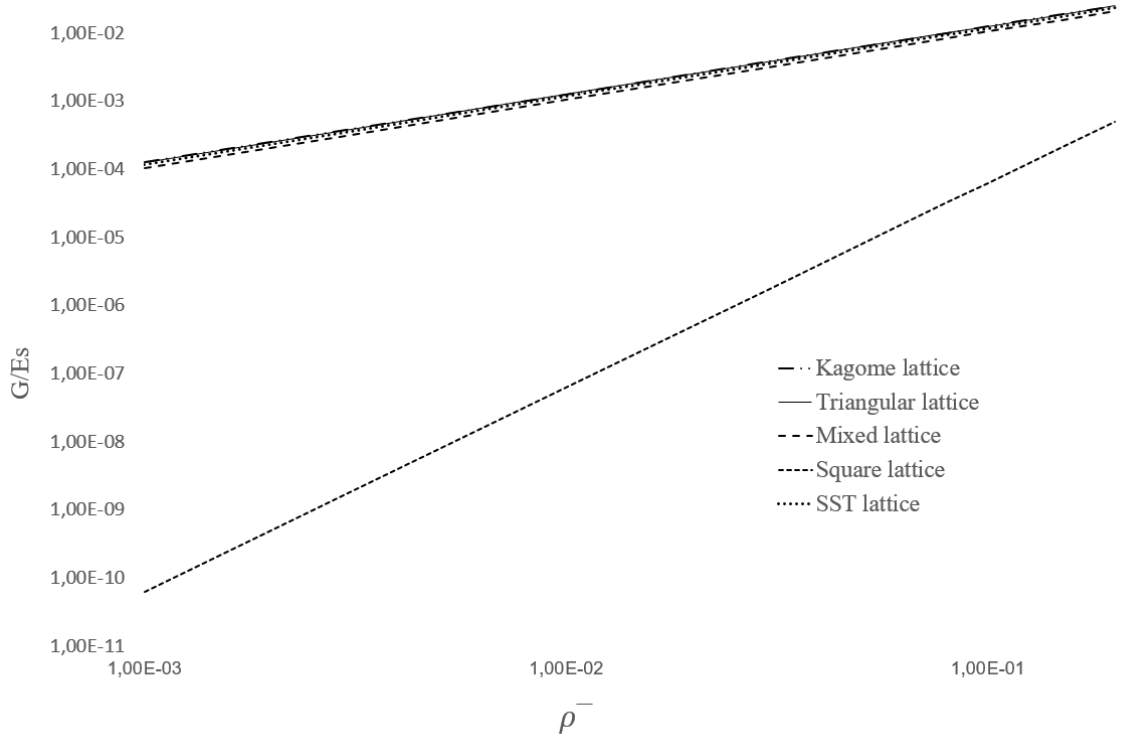

Figure 5.20: Comparative plot of the normalized shear modulus as a function of relative density for SST and other lattices. The square lattice is found to be inferior to those of the SST, mixed, triangular and kagome lattices.

The in-plane shear strength of other stretching dominated lattices and the SST periodic cell is plotted as a function of the relative density, as shown in Figure 5.21. Unfortunately, the elastic

shear buckling property of the other known lattices is not investigated in this work because no previous research and related details were found for this particular property. So only the shear buckling strength of the SST lattice is plotted in the Figure.

As shown in Figure 5.21, the lines indicating the plastic shear yielding properties of the kagome and triangular lattice topologies lie exactly on top of each other, indicating that these lattices have the same property under shear stress. Moreover, these lattices are the strongest compared to others. Unlike that, the square lattice is the weakest lattice among others in terms of plastic shear yielding strength and it has a different slope because it is a bending dominated lattice. The SST lattice material has a similar value of plastic shear yield strength compared to the mixed lattice. More precisely, the SST lattice is slightly stronger than these lattices.

In plastic yielding region of the plot, where the plastic yielding mode of the lattice dominates, we can conclude that the kagome and triangular are superior, in which both having the same yield strength properties. The square lattice is found to be inferior to those of these lattices, although its yield strength property is lower than the triangular and kagome lattices.

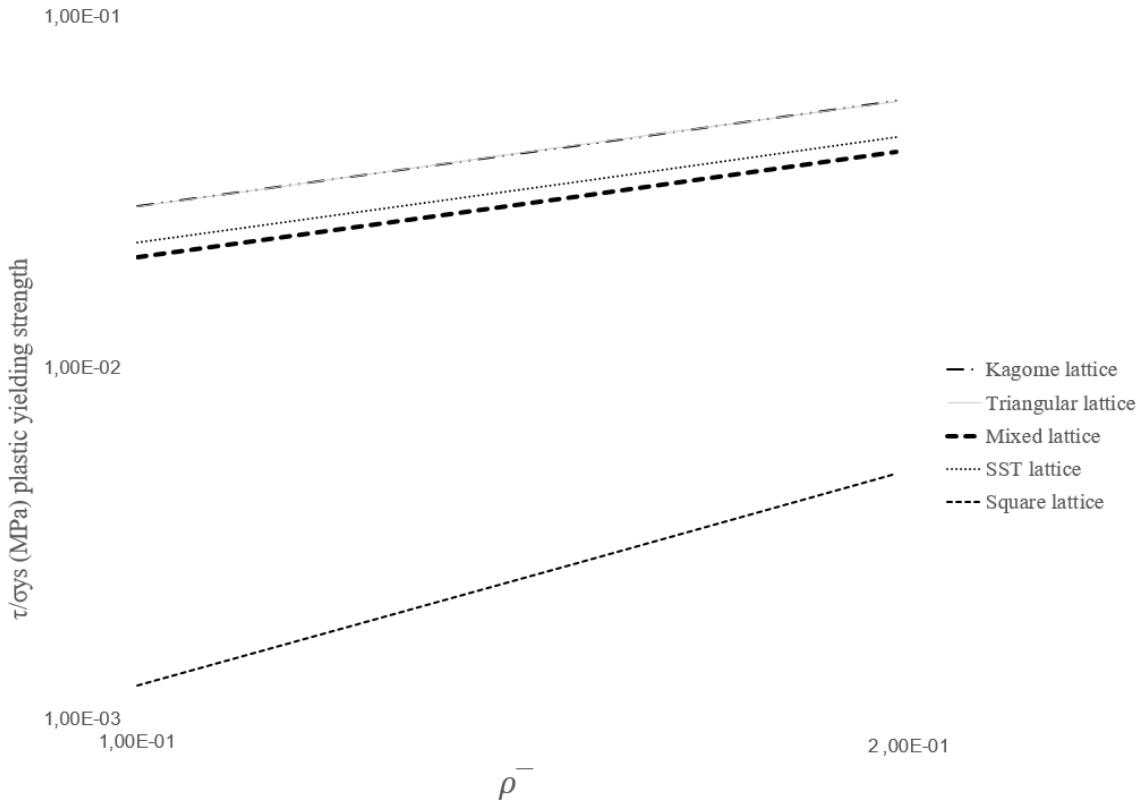

Figure 5.21: Comparative plot of the normalized plastic shear yielding strength as a function of relative density for SST and other lattices.

6 Concluding Remark

The work focused on the study of the in-plane mechanical properties of the SST lattice structure as a function of the relative density of 0.001 to 0.2 under the two different cases of axial and shear stress. This study was carried out using the two different methods, including analytical modelling and FEA simulation.

The mechanical properties of the SST lattice were analytically expressed in the dimensionless equations based on truss and simple beam theories. The analytical method was used to obtain a precise dimensionless equation for the in-plane mechanical properties of the perfect SST topology. The outcome of the analytical investigation of the elasticity modulus and shear modulus of the SST lattice exhibited that the structure was dictated by the stretching dominated deformation mechanism under tensile and shear stresses. The investigation of the SST tessellation under axial compressive stress was also performed. The results depicted that at low values of relative density the bars are very slender $t << l$, which led to the lattice elements experiencing the elastic buckling behaviour, so that the axial compressive force in the bar became equal to the Euler buckling load. Therefore, the SST lattice was exposed to the bending dominated mechanism in the region of elastic buckling strength, where the strength was scaled on $\bar{\rho}^3$. However, at higher values of relative density the bars were chunkier. After exceeding the critical density point, the axial compressive stress in the bar reaches the yield strength of the material, which is known as plastic yielding. Therefore, the SST lattice subjected to the deformation of the stretching dominated mechanism in the region of plastic yield strength, where the strength was scaled on $\bar{\rho}^1$. The SST lattice had a similar mechanical behaviour to the above mentioned idea in case of shear buckling and yield strength.

The SST unit cell was examined using the FEA simulation method to verify the results obtained from the analytical study. The commercial software Abaqus CAE is employed to perform the FEA simulations to study the elastic modulus, compressive strength, shear modulus and shear strength characteristics of the SST cell wall. For this purpose, all nodal constraint equations and the corresponding boundary condition and prescribed displacements have been carefully implemented. The simulation showed a reasonable result because the bars in the unit cell were uniformly loaded and the unit cell had two symmetry plans. In comparison, the results obtained exhibited that the two methods were in good agreement and well matched, which means that they are reliable techniques for studying of the in-plane mechanical properties for further research.

Furthermore, the analytical result of the SST lattice topology was compared with the other stretching dominated lattices, with the following remarkable conclusion:

- The relative density constant of the SST lattice was relatively lower than that of the Mixed and triangular lattices, for a given value of t/l the SST cell wall was much lighter than the kagome and triangular lattices and heavier than the kagome and square lattices.

- The square lattice cell had the highest elastic modulus value and was found to be superior compared to the others and the SST cell had the lowest stiffness value among the others stretching dominated lattices.
- In the elastic compressive buckling strength region, the mixed and triangular lattice topologies had the lowest buckling strength, while the kagome was the strongest. The SST lattice is much weaker than the kagome cell and much stronger than the mixed and triangular lattice topologies.
- In the plastic compressive yielding strength region, the kagome and square cells were the strongest lattices while the SST unit cell was the weakest of these lattices.
- The kagome and triangular lattice cells had the higher shear modulus and the square lattice topology had the lowest shear modulus property among the others. The square lattice had a different slope compared to the others indicating it was a bending dominated lattice. The SST lattice showed an approximately similar shear modulus compared to the triangular, mixed and kagome tessellations.
- Finally, in the plastic shear yielding region, the kagome and triangular lattice topologies were superimposed exactly on top of each other and these cell lattices were the strongest compared to others. The square lattice was the weakest lattice among others and had a different slope because it was a bending dominated lattice. The SST lattice material had a similar plastic shear yield strength value compared to the mixed lattice. More precisely, the SST lattice was superior compared to the square and mixed cells.

7 Recommendation for Future Work

The two methods used in this paper provided an excellent basis to investigate the SST lattice. These methods showed reliable results for the in-plane mechanical properties of the lattice under axial and shear stresses. Nevertheless, future work is needed to improve the reliability of this study. The experimental method could be used to further investigation the in-plane mechanical property of the lattice and to increase the reliability of the study in the future.

Unfortunately, the elastic shear buckling property of the other known lattices is not investigated in this work because no previous studies and related details have been found for this particular property. Therefore the results obtained for the SST lattice could be compared with other lattices in future work.

The FEA method could be improved in future studies by checking the quality of the mesh as this will help to improve the accuracy of the results obtained. Moreover, the reliability of the FEA method could be increased by rationally obtaining the increments. This is because the choice of suitable increments leads to higher accuracy of the convergence study.

8 References

Branko Grünbaum, Geoffrey Colin Shephard and Dover Publications (2019). *Tilings and patterns*. Mineola, New York: Dover Pubications, Inc.

Cabras, L. and Brun, M. (2014). Auxetic two-dimensional lattices with Poisson's ratio arbitrarily close to −1. *Proceedings of the Royal Society A: Mathematical, Physical and Engineering Sciences*, 470(2172), p.20140538.

Chopra, P. (2009). Effective mechanical properties of lattice materials. *Library.ubc.ca*. [online] Available at: https://open.library.ubc.ca/cIRcle/collections/ubctheses/24/items/1.0072404.

Critchlow, K. (2000). *Order in space*. London: Thames & Hudson.

Davies, J.M. (2015). *Lightweight sandwich construction.* John Wiley.

Deshpande, V.S., Ashby, M.F. and Fleck, N.A. (2001). Foam topology: bending versus stretching dominated architectures. *Acta Materialia*, 49(6), pp.1035–1040.

Fan, H., Jin, F. and Fang, D. (2009). Uniaxial local buckling strength of periodic lattice composites. *Materials & Design*, 30(10), pp.4136–4145.

Fleck, N.A., Deshpande, V.S. and Ashby, M.F. (2010). Micro-architectured materials: past, present and future. *Proceedings of the Royal Society A: Mathematical, Physical and Engineering Sciences*, 466(2121), pp.2495–2516.

Gibson, L.J. and Ashby, M.F. (2010). *Cellular solids : structure and properties*. Cambridge: Cambridge Univ. Press.

Gomez-Jauregui, V., Otero, C., Arias, R. and Manchado, C. (2012). Generation and Nomenclature of Tessellations and Double-Layer Grids. *Journal of Structural Engineering*, 138(7), pp.843–852.

H Martyn Cundy and Rollett, A.P. (2007). *Mathematical models*. St. Albans: Tarquin Publications.

Hutchinson, R.G. and Fleck, N.A. (2006). The structural performance of the periodic truss. *Journal of the Mechanics and Physics of Solids*, 54(4), pp.756–782.

Maxwell, J.C. (1864). L. On the calculation of the equilibrium and stiffness of frames. *The London, Edinburgh, and Dublin Philosophical Magazine and Journal of Science*, 27(182), pp.294–299.

Pellegrino, A.S. and Calladine, C.R. (1984). *Matrix analysis of statically and kinematically indeterminate frameworks*. Editorial: Cambridge: Cambridge University Engineering Department.

S Krenk and Høgsberg, J. (2016). *Statics and mechanics of structures*. Dordrecht: Springer.

Zok, F.W. (2019). Integrating lattice materials science into the traditional processing–structure–properties paradigm. *MRS Communications*, 9(4), pp.1284–1291.

Appendix 1. Structural Calculation of Uniaxial Forces

As Figure 3.2 shows, due to symmetry (the two dashed white lines) there are only 5 unknown bars, which are marked here $1-5$. The bars that are not marked bend so that they make a negligible contribution compared to the other, which are either in axial tension or axial compression.

To solve the system, 5 equations are needed.

1. Sum of the forces in X and Y at node g.

Assuming that all bars are under axial tension, a positive value for T_2 means tension and a negative value means axial compression. Using this convention, the equations would become as follows:

In X direction:

$$-T_4 - T_2 Cos\ 60 + T_3 Cos\ 60 = 0 \quad (1.1)$$

In Y direction:

$$-T_1 + T_3 Cos\ 30 + T_2 Cos\ 30 = 0 \quad (1.2)$$

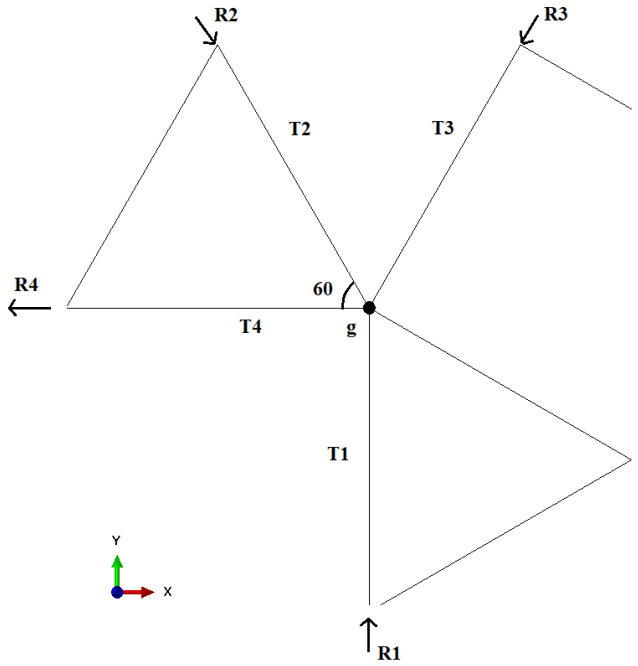

2. Sum of the force in X at node m.

Again with the assumption that all bars are under axial tension.

In X direction:

$$T_5 + 2\,T_3 Cos\,60 = 0 \qquad (1.3)$$

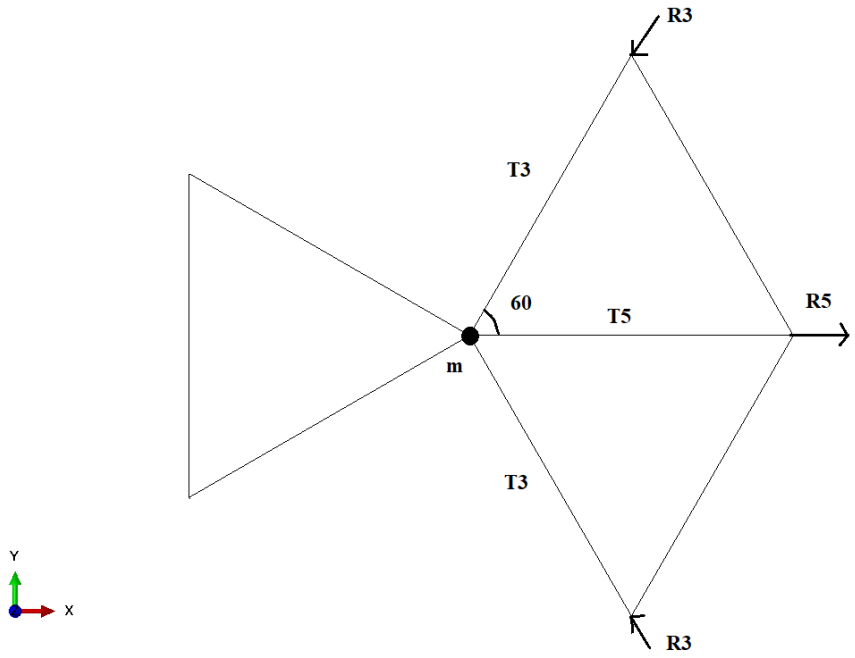

3. The sum of the forces on the upper (or lower surfaces) is equal to σbW.

$$T_1 + T_3 Cos\,30 + T_2 Cos\,30 = -\sigma bW/2 \qquad (1.4)$$

4. The last equation is more complicated; it should be based on the deformation of the unit cell. The last equation is based on the deformation of the bars in a triangle $(2,3,5)$. The deformed shape is shown with dashed lines.

All bars have a length l and the extension of a bar is Δl_i . Therefore, Δx and Δy must to be expressed as a function of $\Delta l_{1,2,3,4,5}$ to have a final equation.

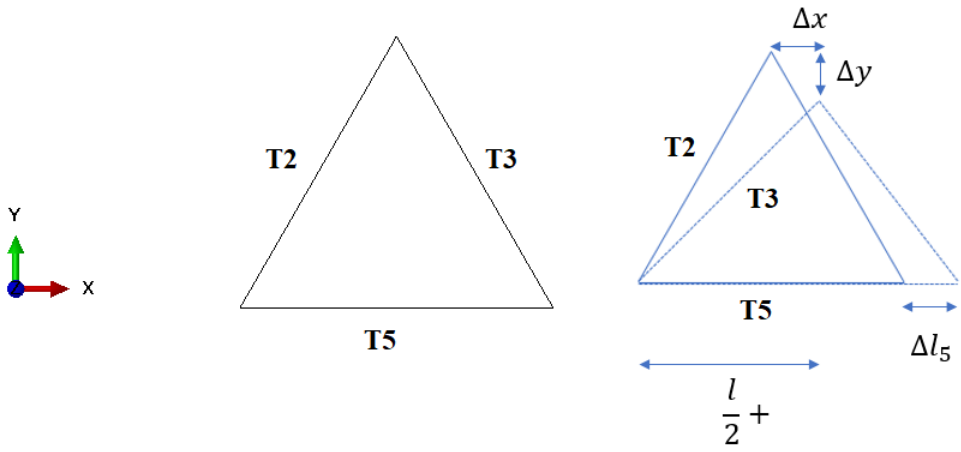

Taking into account the deformed triangle from the left side, the following equation is obtained:

$$(\frac{l}{2}+\Delta x)^2+(h-\Delta y)^2=(l+\Delta l_2)^2 \tag{1.5}$$

Looking at the deformed triangle from the right side, the following equation results:

$$(\frac{l}{2}+\Delta l_5-\Delta x)^2+(h-\Delta y)^2=(l+\Delta l_3)^2 \tag{1.6}$$

The two equations $(A.3)$ and $(A.4)$ can be used to eliminate $(h-\Delta y)^2$, resulting in the following equation:

$$(l+\Delta l_2)^2-\left(\frac{l}{2}-\Delta x\right)^2=(l+\Delta l_3)^2-\left(\frac{l}{2}+\Delta l_5-\Delta x\right)^2 \tag{1.7}$$

Where $\propto = \Delta l_5-\Delta x$

$$l^2+2l\Delta l_2-{\Delta l_2}^2-\left(\frac{l^2}{4}+l\Delta x+\Delta x^2\right)=l^2+2l\Delta l_3-{\Delta l_3}^2-\left(\frac{l^2}{4}+l\propto+\propto^2\right) \tag{1.8}$$

By neglecting second order terms $\Delta x^2\cong\Delta y^2\cong{\Delta l_i}^2\cong 0$

$$2l\Delta l_2-l\Delta x=2l\Delta l_3-l\propto \tag{1.9}$$

$$2\Delta l_2-\Delta x=2l\Delta l_3-\Delta l_5+\Delta x \tag{1.10}$$

$$2\Delta l_2+\Delta l_5=2\Delta l_3+2\Delta x \tag{1.11}$$

$$\frac{2\Delta l_2}{l}+\frac{\Delta l_5}{l}=\frac{2\Delta l_3}{l}+\frac{2\Delta x}{l} \tag{1.12}$$

$$2\varepsilon_2+\varepsilon_5=2\varepsilon_3+\varepsilon_4 \tag{1.13}$$

$$2T_2+T_5=2T_3+T_4 \tag{1.14}$$

Appendix 2. Virtual Work Calculation of Axial Displacement

According to the definition of virtual work, for all systems based on virtual forces and stresses, the total internal work is equal to the total external force. The virtual work for trusses is defined as follows (S Krenk and Høgsberg, 2016):

$$\sum_{Joints} \delta u_j{}^T T_j = \sum_{Bars} l_i \delta \epsilon_i F_i \tag{2.1}$$

T_j=*External forces at joints*

F_i=*Internal forces at struts*

$\delta u_j = Virtual\ displacement\ of\ joints$

$\delta \epsilon_i = Virtual\ strain\ of\ joints$

$l_i = Length\ of\ each\ bars$

In order to determine the displacement in the y direction, a force in this direction could be added. The internal forces from the actual forces are denoted as $F^o{}_1, \dots, F^0{}_i$ in calculation and the internal forces from the virtual forces are shown as $F^1{}_1, \dots, F^1{}_i$.

The displacement related to T^1 can be defined with the help of the virtual work calculation, if all the bars in the lattice are elastic. The equation below can be changed if the actual loads create a displacement field and the load creates the force field. As there is only one external virtual force acting, the equation is rearranged as follows:

$$u^0 T^1 = \sum_{Bars} l_i \epsilon^0{}_i F^1{}_i \tag{2.2}$$

Where u^0 stands for the displacement in T^1 direction.

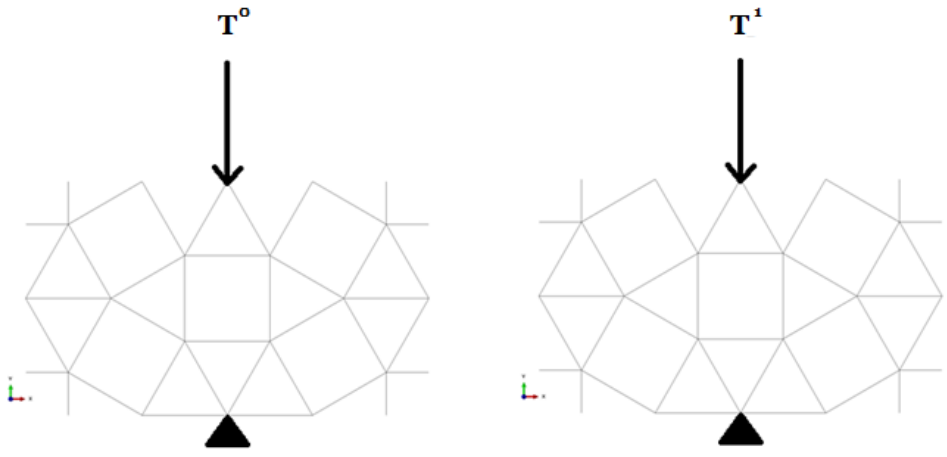

Figure 1: Illustration of virtual force T^0 and actual force T^1

We assume the the magnitude of the virtual force $T^1 = 1$, which gives the following formulae:

$$u^0 = \sum_{Bars} \frac{l_i}{(EA)_i} {F^1}_i {F^0}_i \tag{2.3}$$

The equation below is correct to determine the displacement of the nodes at the tope surface of the lattice. The internal forces of virtual forces can be determined by calculating the internal forces of external forces because they act in at the same direction and at the same joints.

$$u^0 = \sum_{Bars} \frac{l_i}{(EA)_i} {T^1}_i {T^0}_i \tag{2.4}$$

Using the result obtained in Table B and inserting it into Equation $B.4$ the displacement in the direction of T^1 is determined as the following:

$$u = \frac{0.654\ lT}{E_s A} \tag{2.5}$$

Table 2: Calculation of the required elements of the lattice to achieve uniaxial displacement.

Bars	Length of Strut	F^0	F^1	$\frac{lT}{E_s A}$
so	$l/2$	$-0.25T$	-0.25	0.03125
td	$l/2$	$-0.25T$	-0.25	0.03125
ve	$l/2$	$-0.25T$	-0.25	0.03125
yl	$l/2$	$-0.25T$	-0.25	0.03125
fx	l	$-0.25T$	-0.25	0.0625
gz	l	$-0.25T$	-0.425	0.0625
sh	$l/2$	$0{,}0241\,T$	0,0241	0.00029
ud	$l/2$	$0{,}0241\,T$	0,0241	0.00029
yi	$l/2$	$0{,}0241\,T$	0,0241	0.00029
er	$l/2$	$0{,}0241\,T$	0,0241	0.00029
fg	l	$0{,}0241\,T$	0,0241	0.00058
zx	l	$0{,}0241\,T$	0,0241	0.00058
gb	l	$-0{,}1203\,T$	-0,1203	0.0145
em	l	$-0{,}1203\,T$	-0,1203	0.0145
my	l	$-0{,}1203\,T$	-0,1203	0.0145
zq	l	$-0{,}1203\,T$	-0,1203	0.0145
xw	l	$-0{,}1203\,T$	-0,1203	0.0145
ms	l	$-0{,}1203\,T$	-0,1203	0.0145
nd	l	$-0{,}1203\,T$	-0,1203	0.0145
fc	l	$-0{,}1203\,T$	-0,1203	0.0145
ag	l	$-0{,}1684\,T$	-0,1684	0.0284
af	l	$-0{,}1684\,T$	-0,1684	0.0284
pz	l	$-0{,}1684\,T$	-0,1684	0.0284
xp	l	$-0{,}1684\,T$	-0,1684	0.0284
ej	l	$-0{,}1684\,T$	-0,1684	0.0284
jv	l	$-0{,}1684\,T$	-0,1684	0.0284
kd	l	$-0{,}1684\,T$	-0,1684	0.0284
ks	l	$-0{,}1684\,T$	-0,1684	0.0284
pq	l	$0{,}1203\,T$	0,1203	0.0145
wq	l	$0{,}1203\,T$	0,1203	0.0145
mj	l	$0{,}1203\,T$	0,1203	0.0145
kn	l	$0{,}1203\,T$	0,1203	0.0145
$\sum Sum$				$0.0145\frac{lT}{E_s A}$

Appendix 3. Structural Calculation of Shear Forces

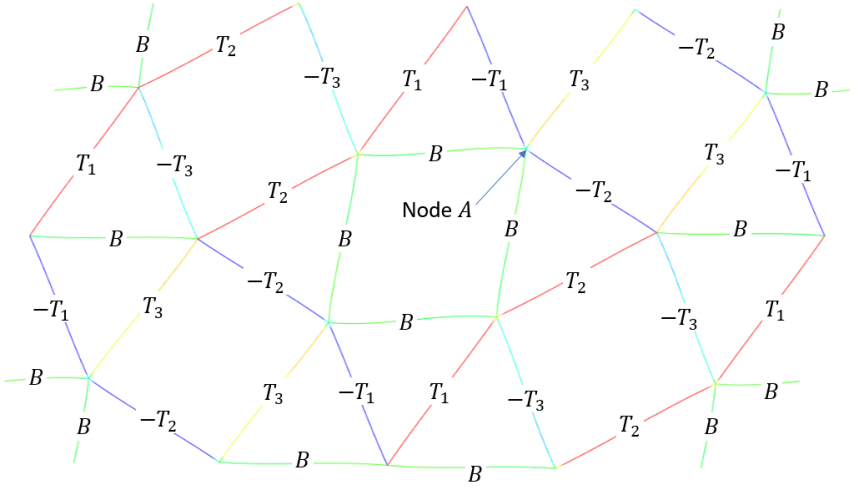

Figure 2: In shear, there are three unknowns: T_1, T_2, T_3. (we can neglect the contribution of the bars in bending, labelled B.)

First, the sum of the forces at node A is obtained:

$$\Sigma F_x = T_1 \cos 60° - T_2 \cos 30° - T_3 \cos 60° = 0 \tag{3.1}$$

$$\Sigma F_y = -T_1 \sin 60° + T_2 \sin 30° - T_3 \sin 60° = 0 \tag{3.2}$$

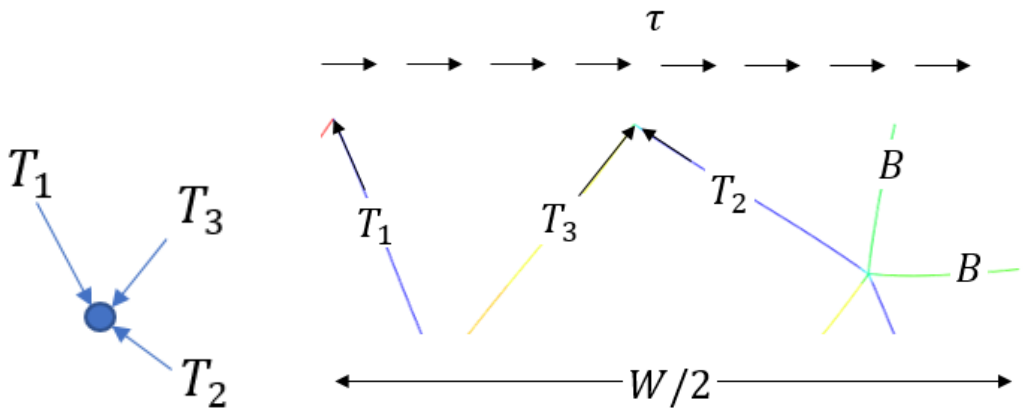

Secondly, the boundary condition gives:

$$\Sigma F_x = -T_1 \cos 60° - T_2 \cos 30° + T_3 \cos 60° = \tau b W \tag{3.3}$$

Appendix 4. Virtual Work Calculation of Shear Displacement

Table 4: Calculation of the required elements of the lattice for determining shear displacement.

Bars	*Length of Strut*	F^0	F^1	$\frac{lT}{E_sA}$
T_1	l	*-0.3333 T*	*-0.3333*	0.1111
T_1	l	*-0.3333 T*	*-0.3333*	0.1111
T_1	l	*-0.3333 T*	*-0.3333*	0.1111
T_1	l	*-0.3333 T*	*-0.3333*	0.1111
$-T_1$	l	*0.3333 T*	*0.3333*	0.1111
$-T_1$	l	*0.3333 T*	*0.3333*	0.1111
$-T_1$	l	*0.3333 T*	*0.3333*	0.1111
$-T_1$	l	*0.3333 T*	*0.3333*	0.1111
T_2	l	−0,2887 *T*	−0,2887	0.0833
T_2	l	−0,2887 *T*	−0,2887	0.0833
T_2	l	−0,2887 *T*	−0,2887	0.0833
T_2	l	−0,2887 *T*	−0,2887	0.0833
$-T_2$	l	0,2887 *T*	0,2887	0.0833
$-T_2$	l	0,2887 *T*	0,2887	0.0833
$-T_2$	l	0,2887 *T*	0,2887	0.0833
$-T_2$	l	0,2887 *T*	0,2887	0.0833
T_3	l	−0,1666 *T*	−0,1666	0.0278
T_3	l	−0,1666 *T*	−0,1666	0.0278
T_3	l	−0,1666 *T*	−0,1666	0.0278
T_3	l	−0,1666 *T*	−0,1666	0.0278
$-T_3$	l	0,1666 *T*	0,1666	0.0278
$-T_3$	l	0,1666 *T*	0,1666	0.0278
$-T_3$	l	0,1666 *T*	0,1666	0.0278
$-T_3$	l	0,1666 *T*	0,1666	0.0278
$\sum$ *Sum*				$1.7775\frac{lT}{E_sA}$

Using the result obtained in the Table D and inserting to Equation $D.1$ gives the shear displacement as the following:

$$u = \sum_{Bars} \frac{l_i}{(EA)_i} T^1{}_i T^0{}_i \qquad u = \frac{1.7775\ lT}{E_sA} \tag{4.1}$$